# Molybdenum(III) Thiocyanate- and Selenocyanate-Based One-Dimensional Heteronuclear Polymers: Coordination Affinity-Controlled Assemblage of Mixed Spin and Mixed Valence Derivatives with Ni(II) and Co(II/III)

Maliheh Mousavi, Carine Guyard-Duhayon, Kateryna Bretosh, Virginie Béreau, Jean-Pascal Sutter

▶ **To cite this version:**

Maliheh Mousavi, Carine Guyard-Duhayon, Kateryna Bretosh, Virginie Béreau, Jean-Pascal Sutter. Molybdenum(III) Thiocyanate- and Selenocyanate-Based One-Dimensional Heteronuclear Polymers: Coordination Affinity-Controlled Assemblage of Mixed Spin and Mixed Valence Derivatives with Ni(II) and Co(II/III). Inorganic Chemistry, 2020, 59 (11), pp.7603-7613. 10.1021/acs.inorgchem.0c00459 . hal-02749318

**HAL Id: hal-02749318**
**https://hal.science/hal-02749318**

Submitted on 10 Nov 2020

**HAL** is a multi-disciplinary open access archive for the deposit and dissemination of scientific research documents, whether they are published or not. The documents may come from teaching and research institutions in France or abroad, or from public or private research centers.

L'archive ouverte pluridisciplinaire **HAL**, est destinée au dépôt et à la diffusion de documents scientifiques de niveau recherche, publiés ou non, émanant des établissements d'enseignement et de recherche français ou étrangers, des laboratoires publics ou privés.

# Molybdenum(III) Thiocyanate- and Selenocyanate-Based 1D-Heteronuclear Polymers: Coordination Affinity-Controlled Assemblage of Mixed Spin and Mixed Valence Derivatives with Ni(II) and Co(II/III)

Malihe Mousavi,[a] Carine Duhayon,[a] Kateryna Bretosh,[a]

Virginie Béreau*[a,b], Jean-Pascal Sutter*[a]

[a] *Laboratoire de Chimie de Coordination (LCC) du CNRS,*

*Université de Toulouse, CNRS, F-31077 Toulouse, France*

[b] *Université de Toulouse, Institut Universitaire de Technologie Paul Sabatier,*

*Département de Chimie, F-81104 Castres, France*

*virginie.bereau@lcc-toulouse.fr

*sutter@lcc-toulouse.fr

## ABSTRACT

1D-coordination polymers constructed with the 4d metallo-ligand $[Mo(NCS)_6]^{3-}$ associated to $Ni^{II}$ and $Co^{II}$ complexes are reported. A first series consist in anionic NCS-bridged $[Mo\text{-}M^{II}]^-$ coordination polymers associated to a discrete paramagnetic complex or a diamagnetic $Co^{III}$ complex acting as cations. The latter takes advantage of the coordination preference of the S-ligand for the soft 3d ions and has led to heterotrimetallic $[Mo^{III}Ni^{II}Co^{III}]$ and mixed valence $[Mo^{III}Co^{II}Co^{III}]$ compounds. A second series concerns neutral chains in which trinuclear $[MoM^{II}_2]$ units are bridged by an additional NCS anion. The soft character of the S atom was also the key to a rare example of a compound involving both high-spin and low-spin $Co^{II}$ centers associated to $[Mo(NCS)_6]$. A [Mo-Ni] derivative obtained with $[Mo(NCSe)_6]^{3-}$ has been considered in order to evaluate the effect of Se versus S on the exchange interaction. The spin distribution for selenocyanate metallo-ligand has been assessed by DFT calculations. The crystal structures for all compounds have been characterized and their magnetic behaviors investigated. These ferrimagnetic systems are characterized by antiferromagnetic Mo-$M^{II}$ interactions in the range of -40 to -90 $cm^{-1}$ (based on $H = -J\boldsymbol{S}_a\boldsymbol{S}_b$ formalism) operative both with $Co^{II}$ and with $Ni^{II}$, thus demonstrating the potential of the $Mo^{III}$-NCS combination for molecular systems in which exchange interactions play an important role.

## INTRODUCTION

The design and rational construction of 1-D coordination polymers has known a revival since it has been shown that such compounds may exhibit slow magnetic relaxation behaviors when favorable conditions are met.[1-4] One of the desirable conditions is a large energy separation between the ground spin state and the states of higher energy, which is obtained when strong exchange interactions take place between the magnetic centers. This has led to involve 4d or 5d metal ions as spin carriers for the design of chains[5-24] because of their spatially more extended valence orbitals (which encompass the magnetic orbitals) that contribute to stronger magnetic interaction between the magnetic centers.[25] These ions can also contribute to the magnetic anisotropy for favorable electronic configurations and geometry.[26-27]

The bridging ligand plays a prominent role in the sign and strength of the magnetic interactions between the metal centers. More generally, the ligands may dictate the geometrical and thereby the magnetic features of the metal center (*ex.* spin state, anisotropy), and contribute to its chemical characteristics such as the assembling preferences for a metallo-ligand. The majority of the reported heterometallic chain systems that involve 4d or 5d metal ions uses the cyanide ligand as bridge between the spin carriers. This ligand efficiently mediates the exchange interactions, moreover many cyanide complexes of 4d and 5d metal ions that can be used as metallo-ligands (building blocks) are known. Comparatively, a very limited number of heteronuclear compounds with other bridging ligands have been reported.[17-18,27-34] Among the possible ligands, thiocyanate ($NCS^-$) is scarcely used in molecular magnetism even if recent examples illustrate its potential for the formation of original coordination polymers.[35-40] This situation is likely resulting from the weak exchange interactions the NCS mediates between 3d ions and the coordination limitations of the S-atom. One exception is in association with $Cr^{III}$ where stronger Cr-NCS-M exchange interactions have been found.[41-43] The efficiency of this bridge when combined to paramagnetic 4d or 5d ions has remained scarcely explored.[44] However, it was shown that associated with the 4d ion $Mo^{III}$, the capability of the thiocyanate ligand to mediate an exchange interaction is greatly increased due to a large spin density delocalization from the metal to the ligand. Antiferromagnetic interactions in the order of -50 $cm^{-1}$ take place with $Ni^{II}$ linked to the S-atom.[40,45] Such a $Mo^{III}$-NCS combination appears therefore very promising for molecular systems in which exchange interactions play an important role. Herein we illustrate this possibility with a series of ferrimagnetic chains involving $[Mo(NCS)_6]^{3-}$ and either $Ni^{II}$ or $Co^{II}$ complexes.

Six original heterometallic chain compounds are reported. In all cases strong antiferromagnetic Mo-Ni and Mo-Co interactions were found to dominate the magnetic behaviors. The versatility of the approach is illustrated by hetero-trimetallic and mixed valence compounds, respectively anionic Mo-$Ni^{II}$ and Mo-$Co^{II}$ chains associated with cationic $Co^{III}$ complexes achieved by taking advantage of the coordination preference of sulfur for soft metal centers. A very original case of chain with $Co^{II}$ centers in different spin-states is also described. Moreover, we examined the effect of replacing thiocyanate with selenocyanate on the exchange interaction in a $Mo^{III}$-$Ni^{II}$ system.

## RESULTS AND DISCUSSION

The chain compounds reported herein are based on $[Mo(NCS)_6]^{3-}$ associated to $Ni^{II}$ or $Co^{II}$ complexes. A first series consists of anionic coordination polymers which charge is compensated either by a paramagnetic $Ni^{II}$ complex or by a diamagnetic $Co^{III}$ complex. These compounds are $[\{Mo(NCS)_6\}\{Ni(en)_2\}]\cdot 0.5[Ni(en)_3]\cdot 0.5\ H_2O$ (**1**), (en stands for 1,2-diaminoethane), $[\{Mo(NCS)_6\}\{NiL^{N4}\}]\cdot 0.5[NiL^{N4}(MeCN)_2]\cdot 0.5CH_3CN\cdot H_2O$ (**2**), ($L^{N4}$ is for the macrocyclic ligand 2,12-dimethyl-3,7,11,1-tetraazabicyclo [11.3.1]-heptadeca-1(17),2,11,13,15-pentaene, Scheme S1 in Supporting Information), $[\{Mo(NCS)_6\}\{NiL^{N4}\}][Co^{III}L^{N4}Br_2]$ (**3**), and $[\{Mo(NCS)_6\}\{Co^{II}L^{N4}\}][Co^{III}L^{N4}Br_2]$ (**4**). Compounds **3** and **4** highlight the coordination preference of the S atom for the softer 3d metal ions $Ni^{II}$ or $Co^{II}$ rather than for $Co^{III}$. A second series comprises neutral chains $[\{Mo(NCS)_6\}\{Co^{II}L^{N4}\}_2(NCS)]\cdot CH_3CN$ (**5**) and $[\{Mo(NCSe)_6\}\{NiL^{N4}\}_2(NCS)]\cdot CH_3CN$ (**6**), in which trinuclear $[MoM_2]$ units are bridged by an additional NCS ligand linking the 3d ions. For the synthesis of **6**, a selenocyanate derivative, $(PPh_4)_3[Mo(NCSe)_6]$, was involved. The crystal structures for all compounds have been characterized and their magnetic behaviors investigated. The spin distribution for $[Mo(NCSe)_6]^{3-}$ has been assessed by DFT calculations.

**Synthesis**. The 1-D coordination polymers **1-6** have been obtained as crystalline solids by inter-diffusion of the corresponding reagents' solutions. For the anionic chains **1** and **2**, the presence of a non-coordinated $Ni^{2+}$ complex acting as cation suggested a possible pathway for magnetic interactions between the chains mediated by this paramagnetic component. Therefore its replacement with a diamagnetic cation has been envisaged. Reaction of $[Mo(NCS)_6]^{3-}$ with $[Ni(en)_2Cl_2]$ or $[NiL^{N4}(H_2O)_2]^{2+}$ in the presence of an excess (5 equiv.) of tetraalkylammonium or $PPh_4^+$ salts failed; crystals of **1** and **2** were systematically obtained as

the only solid product. This lead to consider the diamagnetic $[Co^{III}L^{N4}Br_2]^+$ complex as the diamagnetic cationic counterpart. The reaction of $[Mo(NCS)_6]^{3-}$ and either $[NiL^{N4}(H_2O)_2]^{2+}$ or $[CoL^{N4}(H_2O)_2]^{2+}$ in the presence of $[Co^{III}L^{N4}Br_2]^+$ yielded $[\{Mo(NCS)_6\}\{ML^{N4}\}]\cdot[Co^{III}L^{N4}Br_2]$, **3** (M = $Ni^{II}$) and **4** (M = $Co^{II}$), respectively. The formation of the heterotrimetallic compound **3** and the mixed valence system **4** in which only the $M^{II}$ centers are involved in the coordination polymer whereas the counter-cation is the diamagnetic $Co^{III}$ complex, is supported by the diffraction studies and confirmed by their magnetic behaviors (*vide infra*). This selectivity in the self-sorting process stems from the coordination preference of the S atom for soft 3d centers, that is the metal ion with low oxidation state.[46]

The two neutral chains **5** and **6** have been obtained from the reaction of $[Mo(NC\mathit{Q})_6]^{3-}$ ($\mathit{Q}$ = S, Se) with the 3d complex $[CoL^{N4}(H_2O)_2]^{2+}$ or $[NiL^{N4}(H_2O)_2]^{2+}$ respectively, in the presence of $NCS^-$. A preparation for the $[Mo(NCSe)_6]^{3-}$ was reported earlier but with very poor yields.[47] We now propose a very efficient synthesis (yield > 70 %) of $(NEt_4)_3[Mo(NCSe)_6]$ and $(PPh_4)_3[Mo(NCSe)_6]$.

**Crystal structures**. The molecular crystal structures for compounds **1**-**6** as well as for $(PPh_4)_3[Mo(NCSe)_6]$ have been ascertained by X-ray diffraction experiments on single crystals. ORTEP plots of the asymmetric units with selected bond lengths and angles can be found in the Supporting Information data.

$[\{Mo(NCS)_6\}\{Ni(en)_2\}]\cdot0.5[Ni(en)_3]\cdot0.5H_2O$, **1** (Figure 1), consists in an anionic 1-D coordination polymer made up by $[Mo(NCS)_6]^{3-}$ and $[Ni(en)_2]^{2+}$ units with $[Ni(en)_3]^{2+}$ complexes acting as counter ions, and $H_2O$ molecules located in the lattice. Each $[Mo(NCS)_6]^{3-}$ is connected to two $[Ni(en)_2]^{2+}$ units by two of its $NCS^-$ ligands in *cis* positions and each Ni is linked to two $[Mo(NCS)_6]^{3-}$ units, hence developing into a chain structure along *c* direction. The Ni center has an octahedral coordination sphere with two ethylene diamine ligands and two S atoms from the thiocyanate ligands. The latter belong to two different $[Mo(NCS)_6]^{3-}$ units and are found in coordination sites *cis* to each other. The Ni units are chiral but the two enantiomers alternate in the chain. The NCS-Ni linkage is strongly bent with an angle close to 90° as usually found for the coordination of a sulfur atom, which leads to a zig-zag propagation for the chain. The charge of the coordination polymer is compensated by $[Ni(en)_3]^{2+}$ complexes. Initially these were formed in solution by rearrangement of $[Ni(en)_2Cl_2]$, but much improved yields were reached when preformed $[Ni(en)_3]^{2+}$ was added to the reaction mixture. The crystal packing (Figure S2) shows that the

chains are organized in layers, the $[Ni(en)_3]^{2+}$ and the $H_2O$ solvate molecules are sandwiched between these pseudo-layers. Short separations are found between the chains, these involve non-coordinated sulfur atoms of the thiocyanate ligands with S···S contacts below 4 Å (Figure S2). Such van der Walls interactions could act as pathways for magnetic interactions between the chains because of the spin density carried by the S atoms (*vide infra*).

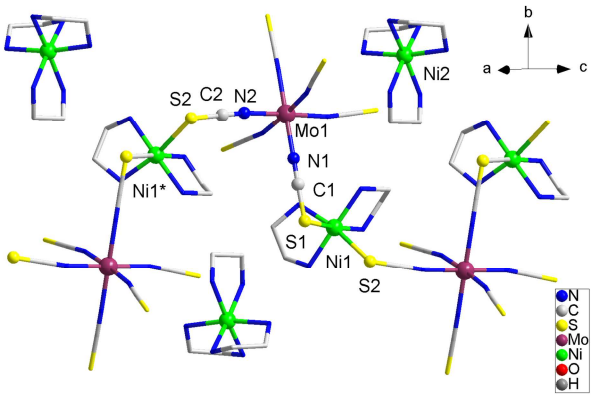


**Figure 1.** Molecular structure of $[\{Mo(NCS)_6\}\{Ni(en)_2\}]\cdot 0.5[Ni(en)_3]\cdot 0.5\ H_2O$, **1**. H atoms and solvate molecules are not shown. For selected bond lengths and angles see Figure S1

The structures for **2**, **3**, and **4**, are built up of very similar chains. $[\{Mo(NCS)_6\}\{NiL^{N4}\}]\cdot 0.5[NiL^{N4}(CH_3CN)_2]\cdot 0.5CH_3CN\cdot H_2O$, **2**, consists in a 1-D assemblage of the two building units $[Mo(NCS)_6]^{3-}$ and $[NiL^{N4}]^{2+}$ with half of independent cationic $[NiL^{N4}(CH_3CN)_2]^{2+}$ complex balancing the charges. Each Mo unit is linked to two $Ni^{2+}$ by two of its $NCS^-$ ligands positioned in *trans*, and each Ni center accommodates in its apical positions two S atoms from two $[Mo(NCS)_6]^{3-}$ units. Because of disorder only inaccurate geometrical parameters were obtained and therefore, they will not be discussed (see the experimental section and Figure S3). The two compounds $[\{Mo(NCS)_6\}\{ML^{N4}\}]\cdot[Co^{III}L^{N4}Br_2]$ with M = $Ni^{II}$ (**3**) or $Co^{II}$ (**4**), are isomorphous. The zig-zag chains are made up by the association of $[Mo(NCS)_6]^{3-}$ and $[M^{II}L^{N4}]^{2+}$, with one $[Co^{III}L^{N4}Br_2]^+$ complex as counter-cation (Figure 2). Like for **2**, in a chain each Mo unit is linked to two $M^{2+}$ by two of its $NCS^-$ ligands positioned in *trans*, and each $M^{2+}$ complex is connected to two $[Mo(NCS)_6]^{3-}$ units by the coordination of two sulfurs in its apical positions. The M-SCN linkages are bent with angles close to 100° (see Figure S4 and S5) whereas the Mo-N-C angles are almost linear, in agreement with the respective coordination of S- and N-atoms. The chains run in parallel along the *c*-direction of the crystal lattice with obvious π-π

stacking between the pyridyl moieties of the $L^{N4}$ ligands from the chains and the $[Co^{III}L^{N4}Br_2]^+$ complexes (Figure S6).

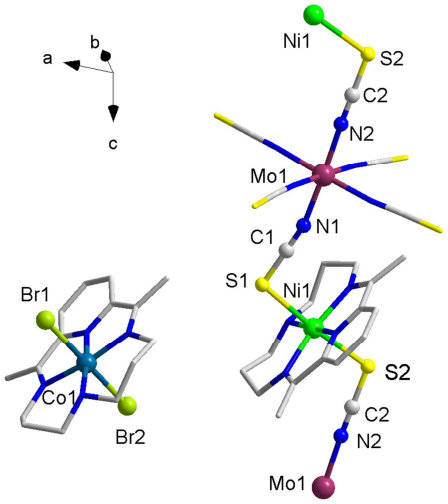


**Figure 2.** $[\{Mo(NCS)_6\}\{NiL^{N4}\}][Co^{III}L^{N4}Br_2]$, **3.** Selected bond lengths and angles can be found in Figure S4.

The structure for $(PPh_4)_3[Mo(NCSe)_6]\cdot CH_3CN$ is very similar to that of $(PPh_4)_3[Mo(NCS)_6]\cdot 2CH_3CN$.[45] The asymmetric unit contains a single molecular unit (Figures 3 and S8). The Mo-N bond lengths are comparable to those for the thiocyanate analogue and the Mo-NCSe linkages are slightly bent with a mean angle of 173.6°. As expected, changing S for Se leads to an increase of the bond length with C as a result of an enlargement of the ionic radius (1.84 Å for $S^{2-}$ and 1.98 Å for $Se^{2-}$).[48] In the crystal lattice, the $[Mo(NCSe)_6]$ units are closely packed with intermolecular Se···Se separations of 3.3757(4) and 3.7502(4) Å; distances close or even below the sum of the ionic radius of Se suggesting contacts between the atoms. These contacts lead to a ladder-type organization of the $[Mo(NCSe)_6]$ units (Figure S9).

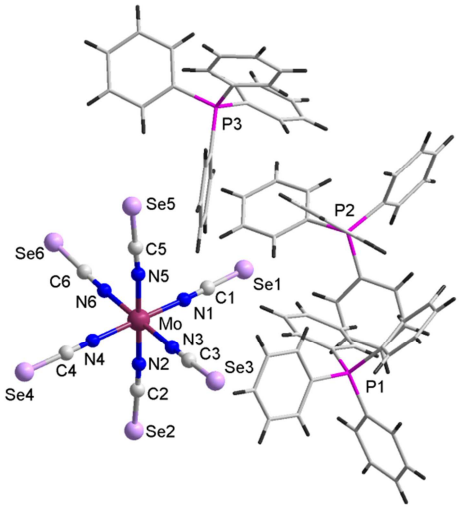


**Figure 3.** Crystal structure for $(PPh_4)_3[Mo(NCSe)_6]\cdot CH_3CN$ (solvate is not depicted).

The two [{Mo(NC$Q$)$_6$}{ML$^{N4}$}$_2$(NCS)]·$CH_3CN$ polymers (M= Co, $Q$ = S for **5**; M = Ni, $Q$ = Se for **6**) are isomorphous and crystallize in the chiral space group $P2_1$. Below we describe the structure of [{Mo(NCSe)$_6$}{NiL$^{N4}$}$_2$(NCS)], **6**, as a representative. The compound consists of trimetallic moieties where two $[NiL^{N4}]^{2+}$ and one $[Mo(NCSe)_6]^{3-}$ units are linked by selenocyanate groups. These [Ni-Mo-Ni] moieties are further interlinked by NCS ligands acting as a bridge between the Ni centers developing thus a 1-D organization along the *b*-axis (Figure 4). One $CH_3CN$ molecule per formula unit is found in the crystal lattice. This structure organization is very similar to that known with the related $[Mo(NCS)_6]$ derivative.[45] The presence of free $NCS^-$ anion in the reaction mixture could have been suspected to lead to ligand exchange with the hexaselenocyanate complex. However, no sign for ligand scrambling (NCS/NCSe) was detected during the structure refinement. This is also supported by the S-Ni bond length (2.552(1) Å) that is very similar to those found for compounds **1-5** whereas the Ni-Se bonds are significantly longer (mean, 2.720 Å). The crystal structure for **5** was investigated at 100 and at 273 K and resulted in very similar shape and bond distances for the Co coordination spheres (see Figure S7).

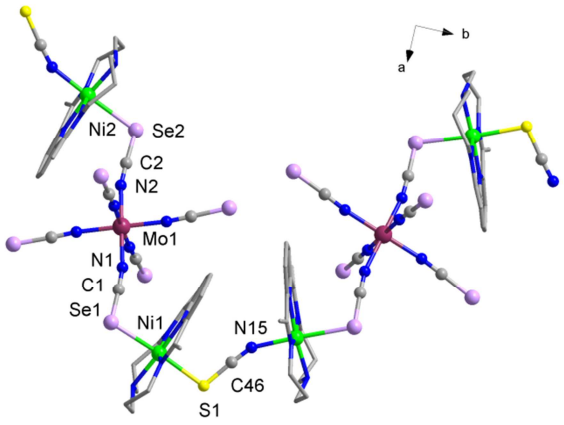


**Figure 4** (left) Molecular structure for [{Mo(NCSe)$_6$}{NiL$^{N4}$}$_2$(NCS)]·$CH_3CN$, **6** (H atoms and solvates are not depicted). For distances and angles see Figure S10.

**Spin density distribution.** The spin density distribution for $[Mo(NCSe)_6]^{3-}$ has been obtained by DFT calculations. Methodology and computational details can be found in the experimental section. The computed spin density distribution and HOMOs for $[Mo(NCSe)_6]^{3-}$ are depicted in Figure 5. Positive density (in grey) localized in the π orbitals is found on the carbon and selenium atoms of the ligands whereas negative spin density (in blue) is observed on the N atoms as a result of spin polarization. The spin populations have been analyzed using the NBO method and are compared to that reported[45] for $[Mo(NCS)_6]^{3-}$ in Table 1 (for details

see Table S1). It can be noticed that replacement of S by Se located just below in the column of the periodic table, has no significant effect on the spin density found on the terminal atom in NC*Q*. This is expected because both NCS and NCSe connect to Mo by the nitrogen atom, therefore the spin transfer proceeding via their orbital overlap should be very similar.

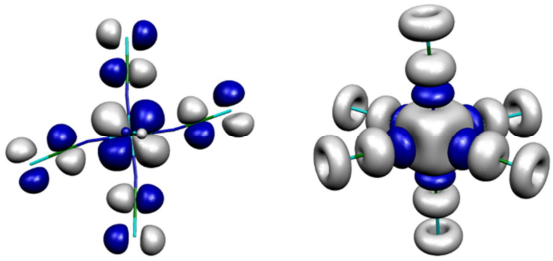

**Figure 5** (left) One of the three HOMOs, and (right) distribution of the spin density (grey: positive, blue: negative) deduced from DFT calculation for $[Mo(NCSe)_6]^{3-}$

**Table 1.** Spin density distribution for $[Mo(NCQ)_6]^{3-}$ (*Q* = S or Se)

| | Total spin density *(mean value in $\mu_B$)* | | | |
|---|---|---|---|---|
| | **Mo** | **N** | **C** | ***Q*** |
| **$[Mo(NCSe)_6]^{3-}$** | 2.474 | -0.081 | 0.100 | Se : 0.069 |
| **$[Mo(NCS)_6]^{3-}$** [45] | 2.515 | -0.077 | 0.091 | S: 0.067 |

## Magnetic properties.

For the discrete complex $[PPh_4]_3[Mo(NCSe)_6]\cdot CH_3CN$ the $\chi_M T = f(T)$ (Figure S11) behavior is in agreement with an isolated S = 3/2 spin state, with values of $\chi_M T$ close to 1.75 $cm^3mol^{-1}K$ between 300 and 50 K, followed by a decrease reaching 0.97 $cm^3mol^{-1}K$ for 2 K. The $Mo^{III}$ is expected to exhibit some Zero Field Splitting (ZFS) that may contribute to the behavior below 50 K. The magnetization recorded at 2 K reaches 2.5 $\mu_B$ for 7 T (Figure S11). The magnetic behavior has been analyzed considering axial ZFS parameter *D* to account for the anisotropy and possible intermolecular interactions using the mean-field approximation (*zJ'*). The variations of $\chi_M T = f(T)$ and $M = f(H)$ have been analyzed simultaneously using PHI software,[49] and best fit was obtained for $g = 1.93$, $D = 3.7 \pm 0.1$ $cm^{-1}$ and $zJ' = -0.117 \pm 0.03$ $cm^{-1}$. These values are very similar to that reported for the $Mo^{III}$-thiocyanate analogue.[45]

For compounds **1**-**6** the temperature dependences of the magnetic susceptibilities are plotted as $\chi_M T = f(T)$ in Figures 6 and 7, and $M = f(H)$ plots are given in Supporting Information. These behaviors underline rather strong antiferromagnetic interactions within the chains. The

overall behavior observed for **1**-**4** (Figure 6) is characteristic for ferrimagnetic chains. The value of $\chi_M T$ at 300 K ($\chi_M T_{300K}$) is below the Curie contributions of the paramagnetic components and steadily decreases as $T$ is lowered, passes a minimum ($\chi_M T_{min}$) before increasing again to reach a maximum ($\chi_M T_{max}$) and eventually drops rapidly as $T$ approaches 2 K. The characteristic data for each compound are gathered in Table X.

**Table 2.** Characteristic data for the magnetic behaviors of **1**-**6**.

| | **1** | **2** | **3** | **4** | **5** | **6** |
|---|---|---|---|---|---|---|
| $\chi_M T_{300K}$[a] | 2.60 | 2.31 | 1.90 | 4.27 | 2.13 | 3.13 |
| $T_{min}$[b] | 40 | 32 | 78 | 88 | – | – |
| $\chi_M T_{min}$[a] | 1.0 | 0.88 | 1.17 | 2.53 | – | – |
| $T_{plat}$[b] | – | – | – | – | 50 | 20 |
| $\chi_M T_{plat}$[a] | – | – | – | – | 0.4 | 0.5 |
| $T_{max}$[b] | – | 15 | 7 | 17 | – | – |
| $\chi_M T_{max}$[a] | – | 0.94 | 2.97 | 3.90 | – | – |
| $\chi_M T_{2K}$[a] | 0.51 | 0.18 | 0.93 | 0.46 | 0.16 | 0.38 |
| $J_{MoM}$[c] | -40.4 | -60.1 | -58.7 | – | -92.0 | -47.16 |

$\chi_M T_{300K}$, $\chi_M T_{min}$ , $\chi_M T_{max}$ and $\chi_M T_{2K}$ refer to the values found respectively , at 300 K, for the first minimum at $T_{min}$, the maximum for $T_{max}$, and the value obtained at 2 K, when reading Figure 6. $\chi_M T_{plat}$ corresponds to the plateau observed and $T_{plat}$. the temperature at which it is reached, when long-range interactions are not operative. ([a]) in $cm^3mol^{-1}K$; ([b]) in K; ([c]) in $cm^{-1}$.

For compound **1**, the value for $\chi_M T_{300K}$ is much below the value of 3.37 $cm^3mol^{-1}K$ anticipated for one S = 3/2 and 1.5×S = 1 (with $g$ = 2.0) in the absence of exchange interactions. This value steadily decreases down to 2 K but the slope shows an inflexion at *ca.* 40 K suggesting that the low $T$ behavior is due to a contribution different from that governing the higher temperature behavior. It can be noticed that the value for $\chi_M T$ at the inflexion is in the order of that expected for an S = ½ resulting from an antiferromagnetic Mo - Ni interaction plus the contribution of half an isolated Ni ion. The absence of the upturn and divergence of $\chi_M T$ anticipated for a ferrimagnetic chain can be attributed to antiferromagnetic interactions between the chains. This $\chi_M T = f(T)$ behavior has been modeled by an expression for an Heisenberg chain of classical spins proposed by Drillon *et al.*[50-51] for a ferrimagnetic system. It is derived from Hamiltonian given in Eq. 1 and remains valid for chains involving single-ion anisotropy.[34] To account for the contribution of the paramagnetic cations present in

**1**, the contribution of half of the S = 1 spin was added. Inter-chain/molecular interactions have been considered in the mean field approximation, which may also account for possible ZFS contributions. Analysis of the experimental behavior between 300 and 20 K yielded $J_{MoNi}$ = -40.4 ± 0.2 $cm^{-1}$; $zJ'$ = -1.2± 0.2 $cm^{-1}$, $g_{Mo}$ = 1.9 (fixed), $g_{Ni}$ = 2.318 ± 0.003. The strength of the antiferromagnetic Mo-Ni interaction is in the order of reported values,[45] and the $zJ'$ parameter confirms the occurrence of inter-molecular exchange interactions.

Eq. 1 $$\hat{H} = \mu_B H \sum_i g_i \hat{S}_i - J \sum_i \hat{S}_i \hat{S}_{i+1}$$

The $\chi_M T$ versus $T$ behavior for **2** is very similar to that of **1** except that the rounded minimum expected for a ferrimagnetic chain is clearly found at *ca* 32 K. This behavior has been reproduced between 15 K and 300 K by the model discussed above with best fit parameters $J_{MoNi}$ = -60.1 ± 0.2 $cm^{-1}$, $g_{Mo}$ = 1.9 (fixed), $g_{Ni}$ = 2.3 (fixed), $zJ'$ = -1.7 ± 0.2 $cm^{-1}$.

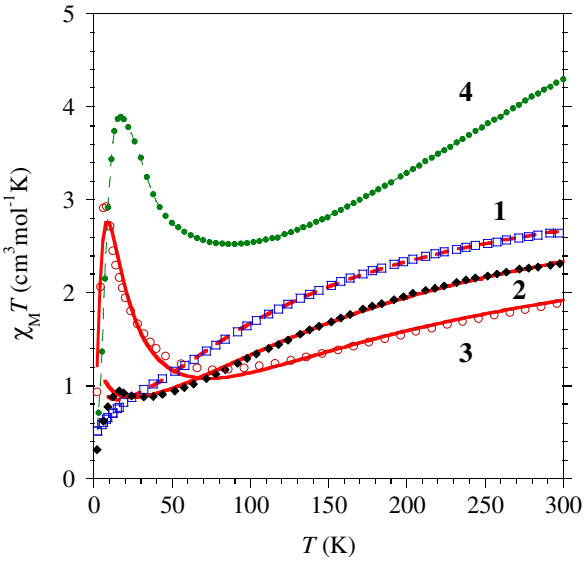


**Figure 6** Experimental and calculated (–) $\chi_M T$ versus $T$ behavior for (□) [{Mo(NCS)$_6$}{Ni(en)$_2$}]·0.5[Ni(en)$_3$], **1**; (◆) [{Mo(NCS)$_6$}{NiL$^{N4}$(MeCN)$_2$}]·0.5[NiL$^{N4}$], **2**; (○) [{Mo(NCS)$_6$}{NiL$^{N4}$}]·[CoL$^{N4}$Br$_2$], **3**; (●) [{Mo(NCS)$_6$}{CoL$^{N4}$}]·[CoL$^{N4}$Br$_2$], **4**. The best fit parameters are discussed in main text.

For [{Mo(NCS)$_6$}{NiL$^{N4}$}]·[Co$^{III}$L$^{N4}$Br$_2$], **3**, and [{Mo(NCS)$_6$}Co$^{II}$L$^{N4}$]·[Co$^{III}$L$^{N4}$Br$_2$]·, **4**, the paramagnetic components are only located in the chains. The $\chi_M T = f(T)$ behaviors show a similar trend to that described above but a clear increase of $\chi_M T$ is found for temperatures below the broad minimum. However, their $\chi_M = f(T)$ behaviors show a maximum respectively at 4.5 and 10 K (Figures S14 and S15), suggesting the occurrence of inter-chain interactions. For **3**, the value for $\chi_M T$ at 300 K is significantly below the Curie contributions for one Mo$^{III}$

and one $Ni^{II}$ center, and the broad minimum exhibited by the curve is found around 80 K. Moreover, the clear but moderate increase of $\chi_M T$ for lower temperatures suggests weaker inter-chain interactions as compared to **2**, thus confirming the effective shielding of the chains by the diamagnetic $Co^{III}$ complexes. The $\chi_M T$ behavior was fairly well reproduced with the Heisenberg chain model by considering alternating S = 1 and S = 3/2 centers, best fit was obtained for $J_{NiMo}$ = -58.7 ± 0.6 $cm^{-1}$; $zJ'$ = -1.67 ± 0.03 $cm^{-1}$, $g_{Mo}$ = 2.1 (fixed), $g_{Ni}$ = 1.96 ± 0.01.

For **4**, the high temperature values for $\chi_M T$ indicate that $Co^{II}$ has high-spin (HS) S = 3/2 configuration with its usual spin-orbit contribution. It is worth noting that this metal center has a low-spin configuration in the precursor complex $[CoL^{N4}(H_2O)_2](ClO_4)_2$[52] ($\chi_M T = f(T)$ between 300 and 2 K is given in Figure S18) This change of the spin state is rationalized by the weaker ligand-field resulting from the S-coordinated thiocyanate in the apical positions. As a result the magnitude of the energy gap between the metal orbitals relative to the mean spin pairing energy is reduced; a situation prone to favor a high spin configuration. This was confirmed for compound **5** discussed below. Albeit this chain is composed only by S = 3/2 spin centers the overall $\chi_M T = f(T)$ behavior is characteristic of a ferrimagnetic system because of the large orbital contribution associated to the $Co^{II}$ units. The lack of an easy to handle theoretical expression for the susceptibility of a chain system involving centers with spin-orbit coupling did prevent from a quantitative analysis of the exchange in **4**. However, the position of the minima in $\chi_M T$ and the value obtained at 300 K evidence strong antiferromagnetic interaction between the $Mo^{III}$ and $Co^{II}_{HS}$.

The field dependence of the magnetization recorded at 2 K (Supporting Information) approaches saturation with 1.68 $\mu_B$ for 5 T. This value is in good accordance with the value given by $g_{Co} \times S_{Co} - g_{Mo} \times S_{Mo}$, *i.e.* 1.5$\mu_B$, based on the *g*-factor in the order of 3[51,53] for HS $Co^{II}$. At 2 K a meta-magnetic like behavior is observed while such an S-shaped curve is no longer found at 10 K. This observation can be correlated with the maximum in $\chi_M$ at 10 K (Figure S15) and reveals sizable inter-chain interactions. AC susceptibility data support possible AF ordering with $T_N$ = 9 K (Figure S15).

From a magnetic view point, $[\{Mo(NCS)_6\}\{CoL^{N4}\}_2(NCS)]\cdot CH_3CN$, **5**, consist of exchange coupled [Co-Mo-Co] units with possible weaker inter-units interaction.[54] The experimental behavior (Figure 7) is in agreement with this picture. The value of $\chi_M T$ at 300 K, and the value reached for the plateau could agree with one Mo (S = 3/2) and either two $Co^{II}_{LS}$ (S = ½) or one $Co^{II}_{HS}$ (S = 3/2) as found in **4** and one $Co^{II}_{LS}$ (S = ½); with expected values of 2.65 and

6.46 $cm^3mol^{-1}K$ in the absence of exchange interactions. However, the experimental behavior could be modeled only when considering a [1/2-3/2-3/2] spin system (Figure 7) whereas fitting did not converge at all when both Co where considered either S = ½ or 3/2. Based on the behavior found in **4**, the high spin configuration is attributed to the $Co^{II}$ with two sulfur-atoms in the apical positions and the low-spin to $Co^{II}$ with one S- and one N-atom in the apical positions. The possibility for a high-spin to low–spin crossover process in the temperature domain 300-50 K can be excluded based on the crystal structure data obtained at 273 and 110 K (Figure S7). Due to the absence of any feature in the variation of $\chi_M T$ between 300 and 20 K, modeling with two exchange parameters did not converge to reasonable results because of the strong correlation between these parameters. Therefore a single exchange parameter $J_{MoCo}$ was considered even if it is unlikely that exchange with HS and LS $Co^{II}$ are same. The possible contributions of the interactions between the $[MoCo_2]$ units[54] and/or ZFS effect of the HS $Co^{II}$ center have been considered within the mean-field approximation (*zj'*). Best fit yielded $J_{MoCo}$ = -92.0 +/-0.2 $cm^{-1}$, *zj*' = -2.40 +/- 0.06 $cm^{-1}$, $g_{Co^{HS}}$ = 2.219 +/- 0.003, $g_{Co^{LS}}$ = 2.0 (fixed), $g_{Mo}$ = 2.0 (fixed) (based on exchange Hamiltonian $H = -J(\mathbf{S}_1\mathbf{S}_2 + \mathbf{S}_2\mathbf{S}_3)$). Here again, a rather strong exchange interaction is evidenced, in agreement with the behaviors discussed above.

$[\{Mo(NCSe)_6\}\{NiL^{N4}\}_2(NCS)]\cdot CH_3CN$, **6**, shows an overall behavior similar to that of **5**. The exchange interactions mainly concerns the trimetallic [Ni-Mo-Ni] unit because interactions between these units through the [Ni-NCS-Ni] linkages are anticipated to be weak, if any.[55] The plateau reached below 20 K is consistent with a S = ½ spin state resulting from antiferromagnetic Mo-Ni interactions. Best fit of the experimental data yields $J_{MoNi}$ = -47.16 ± 0.06 $cm^{-1}$, $g_{Ni}$ = 2.247 ± 0.001 $g_{Mo}$ = 2.0 (fixed), *zJ*' = -0.54 ± 0.01 $cm^{-1}$.

The possibility for slow relaxation of the magnetization for **2**, **4,** and **5** has been probed by AC magnetic susceptibility measurements with and without an applied DC field. No signal was found for the out of phase component, $\chi_M$", of the susceptibility.

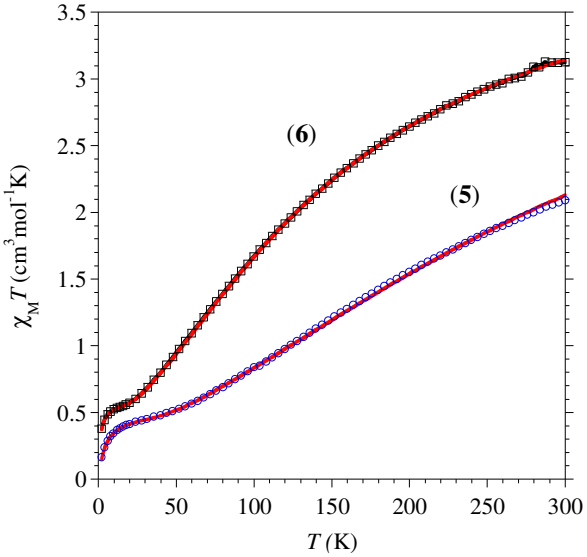


**Figure 7** (a) Experimental and calculated (—) $\chi_M T$ versus $T$ for (○) [{Mo(NCS)$_6$}{CoL$^{N4}$}$_2$(NCS)], **5**, and (□) - [{Mo(NCSe)$_6$}{NiL$^{N4}$}$_2$(NCS)]·, **6**. Best fit parameters are discussed in the text.

The magnetic behaviors exhibited by all the compounds evidence a rather strong antiferromagnetic interaction between Mo$^{III}$ and either Ni$^{II}$ or Co$^{II}$ mediated by the bridging anions. The antiferromagnetic nature of the interaction is due to the NCS-M$^{II}$ angle close to 100° that leads to an overlap of the π-orbitals of the S with the $d_{z2}$ and $d_{x2-y2}$ orbitals of the Ni$^{II}$ and Co$^{II}$ in which unpaired electrons are localized. Since the π-orbitals of the bridging ligand are part of the molecular orbitals (MO) involving the magnetic orbitals of the Mo ion (see Fig 5), the magnetic orbitals of the metals centers share the same MOs and Pauli rule applies.

The exchange interactions found for the Mo-Ni derivatives **1**-**3** are in the order of that reported earlier (-51 cm$^{-1}$)[45] but they show a rather large variation with a strength spanning from -40 cm$^{-1}$ to -60 cm$^{-1}$. This variation seems to parallel the changes in the NCS-Ni angles in these compounds. The smallest angle with 98.3° (mean value) is found in **1** for which $J_{MoNi}$ = -40 cm$^{-1}$, and largest angle is in **2** with 110° (mean value) that also exhibits strongest exchange interaction of the series with $J_{MoNi}$ = -60 cm$^{-1}$. This relationship is supported by the very similar exchange coupling found in **3** and a reported derivative[45] (respectively, -58 and -51 cm$^{-1}$) that both exhibit same NCS-Ni angle of 105.9° (mean value). This trend also applies when the selenocyanate-bridged compound **6** is considered with $J_{MoNi}$ = -47 cm$^{-1}$ for a mean Ni-SeCN angle of 102.4°.

The selenocyanate derivative was considered for evaluating the extent to which the larger Se atom could lead to a more efficient magnetic communication with the Ni ion as a result of better overlap of the valence orbitals of Se with those of Ni$^{II}$. This approach simply follows

what is now well established for the metal ions when changing a 3d for a 4d or a 5d ion.[25] This idea is not novel and some reports suggest indeed an enhanced exchange with the Se,[35,56-58] while others suggest opposite,[59] but effect is usually small. If a sizeable variation of the exchange interaction is induced by moving from S to Se, it should be clearly revealed for Mo-NCSe-Ni system due to the high spin density located on Se. This is not evidenced here. The strength of the Mo-NCSe-Ni interaction in **6**, -47 $cm^{-1}$, is very similar to the Mo-NCS-Ni interaction (-51 $cm^{-1}$) in the isomorphous derivative.[45] The magnetic behavior of **6** therefore suggests that no substantial increase of the exchange interaction may be expected from the use of Se instead of S. This poor modification in the strength of the interaction likely results from the concomitant increase of the Ni-Se bond length with respect to the Ni-S bond length (*i.e.* 2.719 Å versus 2.576 Å respectively in **6** and **5**). The fact $J_{MoNi}$ in **6** is smaller than in **5** is likely related to the slightly more acute NCQ-Ni bridging angle for the former following the trend discussed above.

## CONCLUDING REMARKS

This series of chain compounds highlights the potential and versatility of $[MoNCQ)_6]^{3-}$ ($Q$ = S; Se) as metallo-ligand for the design of heteronuclear coordination polymers with efficient exchange interactions. Both for $Co^{II}$ and $Ni^{II}$, the NCS mediates antiferromagnetic interaction in the order of -30 to -90 $cm^{-1}$ with the 4d ion. Such strong interactions open interesting perspective in the design of strongly correlated ferrimagnetic spin systems. Changing NCS for NCSe was not found to have an effect on the strength of the exchange interaction between the paramagnetic centers.

The marked coordination preferences of the S-ligand for soft 3d metal ions offer unique opportunities for designing original heterotrimetallic and mixed-valence derivatives. The examples reported herein illustrate a facile access to such species with $[Mo(NCS)_6]^{3-}$ using a simple self-sorting reaction.

## EXPERIMENTAL SECTION

All the syntheses were performed under a $N_2$ atmosphere. The chemicals were obtained from commercial sources and used as received. The deoxygenated solvents were prepared by refluxing under a Nitrogen atmosphere. The starting materials $K_3[Mo(NCS)_6]$,[60] $(NEt_4)_3[Mo(NCS)_6]$,[40] $[Ni(en)_2Cl_2]$,[61] $[Ni(en)_3]Cl_2$,[61] $[Co^{II}L^{N4}(H_2O)_2](ClO_4)_2$,[52] $[Co^{III}L^{N4}(Br)_2](ClO_4)$,[62] $[NiL^{N4}(H_2O)_2](ClO_4)_2$[63] were prepared as described in the literature. Elemental C, H and N analyses were performed on a Perkin-Elmer 2400 II analyzer on freshly

prepared and isolated samples. IR spectra were recorded in the 4000-600 $cm^{-1}$ region with a Perkin-Elmer Spectrum 100 FTIR using the ATR mode.

***Synthesis :***

***[{Mo(NCS)$_6$}{Ni(en)$_2$}]·0.5[Ni(en)$_3$]·0.5H$_2$O*** **(1).** Three solutions were successively layered in a Schlenk tube according the following order (from the bottom to the top of the tube): 1) $[Ni(en)_3]Cl_2$ (26 mg; 0.09 mmol) in 10 mL of $H_2O$ 2) $[Ni(en)_2Cl_2]$ (225 mg; 0.9 mmol) in a mixture of 5 mL of EtOH and 5 mL of $H_2O$ and 3) $K_3[Mo(NCS)_6]$ (111 mg; 0.18 mmol) dissolved in 10 mL of EtOH. After one day orange-brown crystals of **1** were collected, and washed with EtOH followed by $Et_2O$. Yield: 45 mg, 33%. Anal. Calcd (%) for $C_{13}H_{28}N_{13}Mo_1Ni_{1.5}S_6 \cdot 0.5H_2O$: C, 20.77; H, 3.89; N, 24.22. Found: C, 21.03; H, 3.54; N, 24.00. IR (ATR): ν ($cm^{-1}$) 3320 (m), 3297 (m), 3250 (m), 2946 (w), 2887 (w), 2103 (m), 2052 (s), 2024 (s), 1569 (m), 1456 (m), 1393 (w), 1366 (w), 1278 (m),1139 (w), 1124 (w), 1097 (m), 1010 (s), 960 (m), 815 (w), 749 (w).

***[{Mo(NCS)$_6$}{NiL$^{N4}$}]·0.5[NiL$^{N4}$(CH$_3$CN)$_2$]·0.5CH$_3$CN·H$_2$O*** **(2).** A solution of $[NiL^{N4}(H_2O)_2](ClO_4)_2$ (61 mg; 0.118 mmol) in 10 mL of $CH_3CN$ was carefully layered on the top of a solution of $(NEt_4)_3[Mo(NCS)_6]$ (100 mg; 0.118 mmol) in 10 mL of $CH_3CN$. Black needles of **2** were collected after one day. Yield: 65 mg, 88 %. Anal. Calcd $C_{28.5}H_{35}N_{12}Mo_1Ni_{1.5}S_6O$: C, 36.49; H, 3.76; N, 17.91. Found: C, 36.93; H, 3.55; N, 17.71. IR (ATR): ν ($cm^{-1}$) 2913 (w), 2041 (s), 1612 (w), 1575 (m), 1420 (m), 1359 (w), 1274 (m), 1262 (m), 1208 (w), 1149 (w), 1059 (w), 1045 (m), 945 (w), 909 (m), 805 (m), 740 (m), 668 (w).

***1D-[{Mo(NCS)$_6$}{NiL$^{N4}$}]·[Co$^{III}$L$^{N4}$Br$_2$]*** **(3).** A solution of $(NEt_4)_3[Mo(NCS)_6]$ (50 mg; 0.059 mmol) and $[Co^{III}L^{N4}(Br)_2](ClO_4)$ (102 mg; 0.177 mmol) in 15 mL of $CH_3CN$ was carefully layered over a solution of $[NiL^{N4}(H_2O)_2](ClO_4)_2$ (30.5 mg; 0.059 mmol) in a mixture of 5 mL of $CH_3CN$ and 5 mL of $H_2O$. Black crystals of **3** were collected after one day. Yield: 40 mg, 57 %. Anal. Calcd. (%) for $C_{36}H_{44}N_{14}Br_2Co_1Mo_1Ni_1S_6$: C, 34.91; H, 3.58; N, 15.83. Found: C, 34.94; H, 3.57; N, 15.76. IR (ATR): ν ($cm^{-1}$) 3210 (w), 30.34 (w), 2914(m), 2291 (w), 2250 (w), 2107 (m), 2051 (s), 1609 (w), 1577 (m), 1460 (w), 1426 (m), 1358 (m), 1307 (w), 1274 (m), 1260 (m), 1214 (m), 1204 (m), 1172 (w), 1143 (m), 1093 (w), 1061 (m), 1009 (m), 937 (m), 910 (m), 891 (m), 815 (m), 751 (w), 662 (w).

***[{Mo(NCS)$_6$}{Co$^{II}$L$^{N4}$}]·{Co$^{III}$L$^{N4}$Br$_2$}*** **(4).** A solution of $(NEt_4)_3[Mo(NCS)_6]$ (50 mg; 0.059 mmol) and $[Co^{III}L^{N4}(Br)_2](ClO_4)$ (102 mg; 0.177 mmol) in 15 mL of $CH_3CN$ was carefully layered over a solution of $[Co^{II}L^{N4}(H_2O)_2](ClO_4)_2$ (31.5 mg; 0.059 mmol) in 5mL of $CH_3CN$

and 5 mL of $H_2O$. Dark brown crystals of **4** were collected after two days. Yield: 50 mg, 66 %. Anal. Calcd. (%) for $C_{36}H_{44}N_{14}Br_2Co_2Mo_1S_6 \cdot CH_3CN$: C, 35.66; H, 3.70; N, 16.41. Found: C, 35.56; H, 3.88; N, 16.48. IR (ATR): ν ($cm^{-1}$) 3309 (w), 31.50 (w), 2911 (m), 2105 (m), 2049 (s), 1576 (m), 1427 (m), 1357(m), 1322 (w), 1309 (w), 1276 (m), 1252 (w), 1211(m), 1143 (m), 1075 (m), 1060 (m), 1038 (m), 1026 (m), 954 (w), 934 (m), 890 (m), 816 (m), 801(m), 752 (m).

**[{Mo(NCS)$_6$}{CoL$^{N4}$}$_2$(NCS)]·CH$_3$CN (5).** $K_3[Mo(NCS)_6]$ (36.1 mg; 0.064 mmol) and KSCN (27.6 mg; 0.284 mmol) were dissolved in 10 mL of $CH_3CN$. This solution was very carefully added above a solution of $[Co^{II}L^{N4}(H_2O)_2](ClO_4)_2$ (70.6 mg; 0.128 mmol) in 10 mL of $CH_3CN$. Dark brown crystals of **5** were collected after a few days. Yield: 52 mg, 69 %. Anal. Calcd (%) for $C_{37}H_{44}N_{15}S_7Mo_1Co_2$: C, 39.08; H, 3.90; N, 18.48. Found: C, 39.22; H, 3,79; N, 18.42. IR (ATR): ν ($cm^{-1}$) 3178 (w), 2912 (w), 2089 (m), 2049 (s), 1569 (w), 1422 (m), 1358 (m), 1323 (m), 1281 (m), 1210 (m), 1147 (m), 1076 (m), 1053 (m), 931 (m), 892 (m), 802 (m), 744 (m).

**(NEt$_4$)$_3$[Mo(NCSe)$_6$]·0.5CH$_3$CN** The synthesis of $(NEt_4)_3[Mo(NCSe)_6]$ has been adapted from a reported procedure.[64] $(NH_4)_3MoCl_6$ (500 mg; 1.37 mmol) was dissolved in 5 mL of $H_2O$ and dropwise added to an aqueous solution of KNCSe (1.58 g; 0.011 mol). The resulting solution was stirred for 1h at room temperature. A small amount of a brown precipitate appeared so the suspension was filtered off and the filtrate was evaporated to dryness. The residue was dissolved in 20 mL of dried MeOH, a pale yellow solution was obtained. $NEt_4Br$ (1.5 g; 7.1 mmol) was added to this solution, immediately a yellow precipitate appeared. After 10 min, the suspension was filtered and the solid washed with 10 mL of MeOH followed be 10 mL of $Et_2O$. Yield: 1.1 g, 72%. Anal. Calcd (%) for $C_{30}H_{60}N_9MoSe_6 \cdot 0.5CH_3CN$: C, 32.74; H, 5,45; N, 11.70. Found: C, 32.44; H, 5,49; N, 11.76. IR (ATR): ν ($cm^{-1}$) 2982 (w), 2035 (s), 1483 (m), 1437 (s), 1392 (w), 1305 (w), 1183 (m), 1173 (m), 1031 (w), 1001 (m), 888 (w), 785 (m), 658 (m).

***(PPh$_4$)$_3$[Mo(NCSe)$_6$]·CH$_3$CN:*** A solution of $(NEt_4)_3[Mo(NCSe)_6]$ (200 mg; 0.179 mmol) in 6 mL of $CH_3CN$ was slowly added to a solution of $PPh_4Cl$ (2 g; 5.3 mmol) in 50 mL of $H_2O$. A yellow precipitate appeared. The suspension was stirred for 30 min. and filtered. The yellow solid was washed with $H_2O$ followed by EtOH and was dried under vacuum. A first purification of this compound was accomplished by dissolving the crude yellow solid in $CH_3CN$ and by adding this solution into a saturated aqueous solution of $PPh_4Cl$. The resulting

yellow solid was dissolved in hot $CH_3CN$ and the resulting solution was stored in a fridge (4°C) for 1 day allowing the formation of yellow crystals. Yield: 190 mg, 60%. Anal. Calcd. (%) for $C_{78}H_{60}N_6MoP_3Se_6.CH_3CN$: C, 53.83; H, 3.56; N, 5.50. Found: C, 53.73; H, 3.80; N, 5.59. IR (ATR): ν ($cm^{-1}$) 3053 (w), 2046 (s), 1705 (m), 1585 (w), 1483 (m), 1434 (s), 1339 (w), 1316 (w), 1107 (s), 1026 (w), 996 (s), 756 (m), 720 (s), 689 (s).

**$[\{Mo(NCSe)_6\}\{NiL^{N4}\}_2(NCS)]\cdot CH_3CN$ (6).** $(NEt_4)_3[Mo(NCSe)_6]\cdot 0.5CH_3CN$ (100 mg; 0.089 mmol) was dissolved in 9 mL of $CH_3CN$. A solution of $[NiL^{N4}(H_2O)_2](ClO_4)_2$ (91.8 mg; 0.178 mmol) in 10 mL of $CH_3CN$ was carefully layered over the Mo solution. 1mL of an aqueous solution of KSCN (600 mg; 6.18 mmol) was added at the bottom of the flask. After 3 days, orange crystals of **6** were collected. Yield: 43 mg, 33 %. Anal. Calcd. (%) for $C_{37}H_{44}N_{15}S_1Se_6Mo_1Ni_2\cdot CH_3CN$: C, 32.10; H, 3.25; N, 15.36. Found: C, 32.15; H, 2.79; N, 15.34. IR (ATR): ν ($cm^{-1}$) 3195(w), 3066 (w), 2936 (w), 2917 (w), 2866 (w), 2735 (w), 2105 (m), 2043(s), 1613 (m), 1580 (m), 1467 (m), 1420 (m), 1384 (w), 1353 (m), 1304 (w), 1270 (m), 1261 (m), 1242 (w), 1203 (m), 1131 (w), 1072 (m), 1044 (m), 1008 (m), 945 (w), 907 (m), 832 (w), 804 (m), 741 (m), 728.1 (w), 664 (m).

***Computational Methodology***: Calculations were performed on the $[Mo(NCSe)_6]^{3-}$ unit found in $(PPh_4)_3[Mo(NCSe)_6]\cdot CH_3CN$ with the atoms' coordinates obtained from the single crystal X-Ray diffraction data. The DFT calculations were performed with the Gaussian03 package,[65] using the unrestricted hybrid B3LYP functional.[66-67] The D95 Dunning-Huzinaga valence double-ζ basis set[68] has been used for C and N atoms whereas the LANL2DZ small-core Hay-Wadt pseudopotential[69-71] has been used for Se and Mo atoms (LAND2DZ keyword in Gaussian). The reported spin densities have been obtained through the Mulliken approach.

***Crystal structures determination***: Crystallographic data for **1**-**6** are given in Table 3. ORTEP are provided as Supporting Information.

**Table 3** Crystallographic Data and Structural Refinement Parameters for **1-6** and $[PPh_4]_3[Mo(NCSe)_6]\cdot CH_3CN$

| | **1** | **2** | **3** | **4** | **5**_100K | **5**_273K | **6** | **$[PPh_4]_3[Mo(NCSe)_6]\cdot CH_3CN$** |
|---|---|---|---|---|---|---|---|---|
| Chemical formula | $C_{26}H_{58}Mo_2N_{26}Ni_3OS_{12}$ | $C_{63}H_{79}Mo_2N_{27}Ni_3O_2S_{12}$ | $C_{36}H_{44}Br_2CoMoN_{14}NiS_6$ | $C_{36}H_{44}Br_2Co_2MoN_{14}S_6$ | $C_{39}H_{47}Co_2MoN_{16}S_7$ | $C_{39}H_{47}Co_2MoN_{16}S_7$ | $C_{39}H_{47}MoN_{16}Ni_2SSe_6$ | $C_{80}H_{63}MoN_7P_3Se_6$ |
| M ($g.mol^{-1}$) | 1503.72 | 1999.30 | 1238.63 | 1238.85 | 1178.18 | 1178.18 | 1459.10 | 1785.05 |
| Crystal system | Monoclinic | Triclinic | Monoclinic | Monoclinic | Monoclinic | Monoclinic | Monoclinic | Triclinic |
| Space group | C2/c | P-1 | $P2_1/c$ | $P2_1/c$ | $P2_1$ | $P2_1$ | $P2_1$ | P-1 |
| *a* (Å) | 28.1182(18) | 10.9968(6) | 14.6508(4) | 14.6700(4) | 10.3237(3) | 10.39890(4) | 10.5795(7) | 12.9876(9) |
| *b* (Å) | 13.8711(5) | 12.2116(7) | 28.7479(7) | 28.7210(6) | 23.3071(7) | 23.46560(5) | 23.6004(14) | 13.1169(10) |
| *c* (Å) | 16.1238(9) | 18.3066(9) | 12.4509(3) | 12.4729(3) | 10.9865(3) | 11.12860(4) | 11.0487(7) | 24.1921(18) |
| $\alpha$ (°) | 90 | 76.0650(18) | 90 | 90 | 90 | 90 | 90 | 95.848(4) |
| $\beta$ (°) | 116.191(7) | 80.8110(19) | 108.009(3) | 107.844(2) | 108.5030(10) | 108.752(4)° | 107.913(3) | 92.688(4) |
| $\gamma$ (°) | 90 | 67.8560(17) | 90 | 90 | 90 | 90 | 90 | 109.917(4) |
| *V* ($Å^3$) | 5643.1(6) | 2203.5(2) | 4987.1(2) | 5002.5(2) | 2506.9(1) | 2571.42(6) | 2624.9(3) | 3839.9(5) |
| *Z* | 4 | 1 | 4 | 4 | 2 | 2 | 2 | 2 |
| $d_{calcd}$ | 1.77 | 1.51 | 1.65 | 1.65 | 1.56 | 1.52 | 1.85 | 1.54 |
| $\mu$ ($mm^{-1}$) | 1.912 | 1.246 | 2.846 | 2.793 | 1.239 | 1.208 | 5.19 | 3.12 |
| T (K) | 180 | 100 | 180 | 180 | 100 | 273 | 110 | 180 |
| Refl. measured | 24185 | 49168 | 58242 | 68256 | 52199 | 69823 | 69381 | 112140 |
| Refl. unique | 7481 | 10937 | 12346 | 12177 | 12330 | 16105 | 18852 | 21006 |
| $R_{int}$ | 0.042 | 0.051 | 0.055 | 0.054 | 0.066 | 0.0615 | 0.029 | 0.031 |
| Refl. with $I > 3\sigma(I)$ | 5105 | 6977 | 8691 | 6380 | 9290 | 10825 | 15575 | 13223 |
| Nb. parameters | 321 | 448 | 550 | 550 | 587 | 587 | 587 | 874 |
| R with $I > 3\sigma(I)$ | 0.0316 | 0.1006 | 0.0866 | 0.0757 | 0.0459 | 0.041 | 0.0538 | 0.0301 |
| Rw with $I > 3\sigma(I)$ | 0.0359 | 0.1266 | 0.0735 | 0.0757 | 0.0496 | 0.048 | 0.0523 | 0.0311 |
| Flack parameter | – | – | – | – | 0.26(2) | 0.09(2) | 0.49(1) | – |
| Residual electron density ($\bar{e}.Å^{-3}$) | 1.31/-0.76 | 3.36/-1.68 | 2.30/-1.65 | 2.59/-2.36 | 1.35/-0.72 | 0.96/-0.51 | 3.65/-1.83 | 1.28/-1.21 |
| CCDC reference | 1938755 | 1938751 | 1938749 | 1938750 | 1938754 | 1983354 | 1938753 | 1938752 |

Intensity data were collected at low temperature on an Oxford Diffraction Gemini/Xcalibur or a Bruker Apex2 using a graphite-monochromated Mo $K_\alpha$ (0.71073 Å) radiation source and equipped with an Oxford Cryosystems Cryostream Cooler Device. Structures were solved using SIR92,[72] SHELXS[73] or SUPERFLIP,[74] and refined by full-matrix least-squares procedures on F using the programs of CRYSTALS.[75] Atomic scattering factors were taken from the International Tables for X-ray Crystallography. When it was possible, all non-hydrogen atoms were refined anisotropically. Hydrogen atoms were refined using a riding model. For **3** and **4**, it was not possible to resolve diffuse electron-density residuals (enclosed solvent molecules). The contribution of the disordered solvent was removed using the SQUEEZE option from PLATON.[76] For **2**, the quality of the collected data was reasonably good however the resulting structure presents a general statistic disorder with high R factors. Measurements on different crystals were performed and despite low temperature (100 K) analyses, the structures always exhibited this general disorder which was rather difficult to treat. The ligand parts of the different moieties have been refined isotropically. Thus no bond distances or angles for this compound can be discussed.

The powder X-ray diffraction pattern was collected for compounds **2**-**5** on a XPert Pro (Theta-Theta mode) Panalytical diffractometer with Lamda (Cu $K_{\alpha1}$, $K_{\alpha2}$) ) 1.54059, 1.54439 Å. They are given in Figure S19.

***Magnetic studies.*** Magnetic measurements were carried out with a Quantum design MPMS 5S SQUID magnetometer. Magnetization data between 2 and 300 K have been obtained in an applied field of 1000 Oe. Isothermal magnetization measurements were performed up to 5 T at 2 K. The *ac* susceptibility responses were recorded using an oscillating field of 3 Oe and a frequency of 1000 Hz in zero-field and with an applied DC field of 1 kOe. The measurements were performed on crushed crystals from freshly isolated samples mixed to grease and held in gelatin capsules. The molar magnetic susceptibilities were corrected for sample holder and for the diamagnetic contribution of all the atoms by using Pascal's tables.

**ACKNOWLEDGEMENTS**

Authors are grateful to Dr. L. Vendier (LCC) for collecting XRPD data, and to MM. J.-F. Meunier and L. Rechignat (LCC) for technical assistance in magnetic data collections.

**ASSOCIATED CONTENT:**

Supporting Information Available: ORTEP plots and additional views for the structural arrangement; bond distances and angle for the compounds; additional magnetic data, powder diffraction diffractograms. CCDC-1938749-1938755, and 1983354 contain the supplementary

crystallographic data for this paper. These data can be obtained free of charge from the Cambridge Crystallographic Data Centre via www.ccdc.cam.ac.uk/data_request/cif.

## REFERENCES


(1) Coulon, C.; Miyasaka, H.; Clérac, R. In *Single-Molecule Magnets and Related Phenomena*; Winpenny, R., Ed.; Springer: Berlin, 2006; Vol. 122, p 163-206.

(2) Gatteschi, D.; Sessoli, R.; Villain, J. *Molecular Nanomagnets*; Oxford University Press: Oxford, 2006.

(3) Lescouëzec, R.; Toma, L. M.; Vaissermann, J.; Verdaguer, M.; Delgado, F. S.; Ruiz-Pérez, C.; Lloret, F.; Julve, M. Design of single chain magnets through cyanide-bearing six-coordinate complexes *Coord. Chem. Rev.* **2005**, *249*, 2691-2729.

(4) Sessoli, R. Record Hard Magnets: Glauber Dynamics Are Key *Angew. Chem. Int. Ed.* **2008**, *47*, 5508-5510.

(5) Pradhan, R.; Desplanches, C.; Guionneau, P.; Sutter, J.-P. Octadecanuclear clusters or 1D polymer with $[\{ML\}_2Nb(CN)_8]_n$ motifs as a function of {ML} (M = Ni, n=6; M = Mn, n = inf.; L = macrocycle) *Inorg. Chem.* **2003**, *42*, 6607-6609.

(6) Toma, L. M.; Toma, L. D.; Delgado, F. S.; Ruiz-Pérez, C.; Sletten, J.; Cano, J.; Clemente-Juan, J. M.; Lloret, F.; Julve, M. trans-dicyanobis(acetylacetonato)ruthenate(III) as a precursor to build novel cyanide-bridged Ru(III)-M(II) bimetallic compounds [M = Co and Ni] *Coord. Chem. Rev.* **2006**, *250*, 2176-2193.

(7) Prins, F.; Pasca, E.; Jongh, L. J. d.; Kooijman, H.; Spek, A. L.; Tanase, S. Long-Range Magnetic Ordering in a $Tb^{III}$–$Mo^{V}$ Cyanido-Bridged Quasi-One-Dimensional Complex *Angew. Chem. Int. Ed.* **2007**, *46*, 6081-6084.

(8) Visinescu, D.; Madalan, A. M.; Andruh, M.; Duhayon, C.; Sutter, J.-P.; Ungur, L.; Van den Heuvel, W.; Chibotaru, L. F. First Heterotrimetallic {3d-4d-4f} Single Chain Magnet, Constructed from Anisotropic High-spin Heterometallic Nodes and Paramagnetic Spacers. *Chem. Eur. J.* **2009**, *15*, 11808 – 11814.

(9) Yoo, H. S.; Ko, H. H.; Ryu, D. W.; Lee, J. W.; Yoon, J. H.; Lee, W. R.; Kim, H. C.; Koh, E. K.; Hong, C. S. Octacyanometalate-based ferrimagnetic $M^{V}Mn^{III}$ (M = Mo, W) bimetallic chain racemates with slow magnetic relaxations *Inorg. Chem.* **2009**, *48*, 5617-5619.

(10) Venkatakrishnan, T. S.; Sahoo, S.; Bréfuel, N.; Duhayon, C.; Paulsen, C.; Barra, A.-L.; Ramasesha, S.; Sutter, J.-P. Enhanced Ion Anisotropy by Nonconventional Coordination Geometry: Single-Chain Magnet Behavior for a $[\{Fe^{II}L\}_2\{Nb^{IV}(CN)_8\}]$ Helical Chain Compound Designed with Heptacoordinate $Fe^{II}$ *J. Am. Chem. Soc.* **2010**, *132*, 6047-6056.

(11) Mikuriya, M.; Yoshioka, D.; Borta, A.; Luneau, D.; Matoga, D.; Szklarzewicz, J.; Handa, M. Molecule-based magnetic materials based on dinuclear ruthenium carboxylate and octacyanotungstate *New J. Chem.* **2011**, *35*, 1226-1233.

(12) Wang, X.-Y.; Avendano, C.; Dunbar, K. R. Molecular magnetic materials based on 4d and 5d transition metals *Chem. Soc. Rev.* **2011**, *40*, 3213.

(13) Freedman, D. E.; Jenkins, D. M.; Long, J. R. Strong magnetic exchange coupling in the cyano-bridged coordination clusters $[(PY_5Me_2)_4V_4M(CN)_6]^{5+}$ (M = Cr, Mo) *Chem. Comm.* **2009**, 4829-4831.

(14) Korzeniak, T.; Desplanches, C.; Podgajny, R.; Gimenez-Saiz, C.; Stadnicka, K.; Rams, M.; Sieklucka, B. Magnetostructural Correlations in $Cu^{II}$-NC-$W^{V}$ Linkage: The Case of $[Cu^{II}(diimine)]^{2+}$-$[W^{V}(CN)_8]^{3-}$ 0D Assemblies *Inorg. Chem.* **2009**, *48*, 2865-2872.

(15) Pedersen, K. S.; Schau-Magnussen, M.; Bendix, J.; H., W.; Palii, A. V.; Klokishner, S. I.; Ostrovsky, S. M.; Reu, O. S.; Mutka, H.; Tregenna-Piggott, P. L. W. Enhancing the blocking temperature in single-molecule magnets by incorporating 3d-5d exchange interactions *Chem. Eur. J.* **2010**, *16*, 13458-13464.

(16) Harris, T. D.; Coulon, C.; Clérac, R.; Long, J. R. Record Ferromagnetic Exchange through Cyanide and Elucidation of the Magnetic Phase Diagram for a $Cu^{II}Re^{IV}(CN)_2$ Chain Compound *J. Am. Chem. Soc.* **2011**, *133*, 123-130.

(17) Martinez-Lillo, J.; Mastropietro, T. F.; De Munno, G.; Lloret, F.; Julve, M. l.; Faus, J. Enhancing the Magnetic Coupling of Oxalato-Bridged $Re^{IV}{}_2M^{II}$ (M = Mn, Co, Ni, and Cu) Trinuclear Complexes via Peripheral Halide Ligand Effects *Inorg. Chem.* **2011**, *50*, 5731-5739.

(18) Martinez-Lillo, J.; Delgado, F. S.; Ruiz Perez, C.; Lloret, F.; Julve, M.; Faus, J. Heterotrimetallic Oxalato-Bridged $Re^{IV}{}_2M^{II}$ Complexes (M = Mn, Co, Ni, Cu): Synthesis, Crystal Structure, and Magnetic Properties *Inorg. Chem.* **2007**, *46*, 3523-3530.

(19) Reczyński, M.; Nowicka, B.; Näther, C.; Kozieł, M.; Nakabayashi, K.; Ohkoshi, S.-i.; Sieklucka, B. Dehydration-Triggered Charge Transfer and High Proton Conductivity in $(H_3O)[Ni^{III}(cyclam)][M^{II}(CN)_6]$ (M = Ru, Os) Cyanide-Bridged Chains *Inorg. Chem.* **2018**, *57*, 13415-13422.

(20) Ru, J.; Zhang, R.-F.; Shi, Y.; Zhang, S.-L.; Li, Q.-L.; Ma, C.-L. Synthesis, structures and magnetic properties of heterobimetallic $Ru^{III}$–3d (3d = Mn, Ni) compounds based on the chiral $Ru^{III}$ building block *New J. Chem.* **2018**, *42*, 16237-16243.

(21) Wei, X.-Q.; Qian, K.; Wei, H.-Y.; Wang, X.-Y. A One-Dimensional Magnet Based on $[Mo^{III}(CN)_7]^{4-}$ *Inorg. Chem.* **2016**, *55*, 5107-5109.

(22) Magott, M.; Tomkowiak, H.; Katrusiak, A.; Nitek, W.; Sieklucka, B.; Pinkowicz, D. Two Cyanide-Bridged $Mn^{II}$–$Nb^{IV}$ Coordination Chain Ferrimagnets Promoted by Interchain Ferromagnetic Interactions *Inorg. Chem.* **2016**, *55*, 5281-5286.

(23) Wei, R.-M.; Cao, F.; Li, J.; Yang, L.; Han, Y.; Zhang, X.-L.; Zhang, Z.; Wang, X.-Y.; Song, Y. Single-Chain Magnets Based on Octacyanotungstate with the Highest Energy Barriers for Cyanide Compounds *Sci Rep* **2016**, *6*, 24372.

(24) Zhang, Y.-Z.; Dolinar, B. S.; Liu, S.; Brown, A. J.; Zhang, X.; Wang, Z.-X.; Dunbar, K. R. Enforcing Ising-like magnetic anisotropy via trigonal distortion in the design of a W(V)-Co(II) cyanide single-chain magnet *Chem. Sci.* **2018**, *9*, 119-124.

(25) Visinescu, D.; Desplanches, C.; Imaz, I.; Bahers, V.; Pradhan, R.; Villamena, F.; Guionneau, P.; Sutter, J. P. Evidence for increased exchange interactions with 5d compared to 4d metal ions. experimental and theoretical insights into the ferromagnetic interactions of a series of trinuclear $[\{M(CN)_8\}^{3-}/Ni^{II}]$ compounds (M = $Mo^{V}$ or $W^{V}$) *J. Am. Chem. Soc.* **2006**, *128*, 10202-10212.

(26) Bar, A. K.; Pichon, C.; Sutter, J.-P. Magnetic anisotropy in two- to eight-coordinated transition–metal complexes: Recent developments in molecular magnetism *Coord. Chem. Rev.* **2016**, *308*, 346-380.

(27) Martínez-Lillo, J.; Faus, J.; Lloret, F.; Julve, M. Towards multifunctional magnetic systems through molecular-programmed self assembly of Re(IV) metalloligands *Coord. Chem. Rev.* **2015**, *289-290*, 215-237.

(28) Larionova, J.; Mombelli, B.; Sanchiz, J.; Kahn, O. Magnetic properties of the two-dimensional bimetallic compounds $(NBu_4)[M^{II}Ru^{III}(ox)_3]$ ($NBu_4$ = tetra-n-butylammonium; M = Mn, Fe, Cu; ox = oxalate) *Inorg. Chem.* **1998**, *37*, 679-684.

(29) Chiozzone, R.; Gonzalez, R.; Kremer, C.; De Munno, G.; Cano, J.; Lloret, F.; Julve, M.; Faus, J. Synthesis, crystal structure, and magnetic properties of tetraphenylarsonium tetrachloro(oxalato)rhenate(IV) and bis(2,2'-bipyridine)tetrachloro(m-oxalato)copper(II)rhenium(IV) *Inorg. Chem.* **1999**, *38*, 4745-4752.

(30) Chiozzone, R.; Gonzalez, R.; Kremer, C.; De Munno, G.; Armentano, D.; Cano, J.; Lloret, F.; M., J.; Faus, J. Heterobimetallic oxalato-bridged Cu(II)Re(IV) complexes. Synthesis, crystal structure and magnetic properties. *Inorg. Chem.* **2001**, *40*, 4242-4249.

(31) Coronado, E.; Galan-Mascaros, J. R.; Gomez-Garcia, C. J.; Martinez-Agudo, J. M.; Martinez-Ferrero, E.; Waerenborgh, J. C.; Almeida, M. Layered Molecule-Based Magnets Formed by Decamethylmetallocenium Cations and Two-Dimensional Bimetallic Complexes $[M^{II}Ru^{III}(ox)_3]_2(M^{II}{}_5$Mn, Fe, Co, Cu and Zn; ox=oxalate) *J. Solid. State. Chem.* **2001**, *159*, 391-402.

(32) Chiozzone, R.; Gonzalez, R.; Kremer, C.; De Munno, G.; Armentano, D.; Lloret, F.; Julve, M.; Faus, J. Heterobimetallic oxalato-bridged M(II)Re(IV) complexes (M=Mn, Fe, Co, Ni): synthesis, crystal structure, and magnetic properties. *Inorg. Chem.* **2003**, *42*, 1064-1069.

(33) Martinez-Lillo, J.; Armentano, D.; De Munno, G.; Wernsdorfer, W.; Julve, M.; Llloret, F.; Faus, J. A heterotetranuclear [NiReIV3] single-molecule magnet *J. Am. Chem. Soc.* **2006**, 14218-14219.

(34) Pedersen, K. S.; Sigrist, M.; Sørensen, M. A.; Barra, A.-L.; Weyhermüller, T.; Piligkos, S.; Thuesen, C. A.; Vinum, M. G.; Mutka, H.; Weihe, H.; Clérac, R.; Bendix, J. $[ReF_6]^{2-}$: A Robust Module for the Design of Molecule-Based Magnetic Materials *Angew. Chem. Inter. Ed.* **2014**, *53*, 1351-1354.

(35) Boeckmann, J.; Wriedt, M.; Näther, C. Metamagnetism and Single-Chain Magnetic Behavior in a Homospin One-Dimensional Iron(II) Coordination Polymer *Chem. Eur. J.* **2012**, *18*, 5284-5289.

(36) Neumann, T.; Ceglarska, M.; Germann, L. S.; Rams, M.; Dinnebier, R. E.; Suckert, S.; Jess, I.; Näther, C. Structures, Thermodynamic Relations, and Magnetism of Stable and Metastable $Ni(NCS)_2$ Coordination Polymers *Inorg. Chem.* **2018**, *57*, 3305-3314.

(37) Suckert, S.; Rams, M.; Germann, L. S.; Cegiełka, D. M.; Dinnebier, R. E.; Näther, C. Thermal Transformation of a Zero-Dimensional Thiocyanate Precursor into a Ferromagnetic Three-Dimensional Coordination Network via a Layered Intermediate *Cryst. Growth Des.* **2017**, *17*, 3997-4005.

(38) Wellm, C.; Rams, M.; Neumann, T.; Ceglarska, M.; Näther, C. Tuning of the Critical Temperature in Magnetic 2D Coordination Polymers by Mixed Crystal Formation *Cryst. Growth Des.* **2018**, *18*, 3117-3123.

(39) Nebbali, K.; Mekuimemba, C. D.; Charles, C.; Yefsah, S.; Chastanet, G.; Mota, A. J.; Colacio, E.; Triki, S. One-Dimensional Thiocyanato-Bridged Fe(II) Spin Crossover Cooperative Polymer With Unusual FeN5S Coordination Sphere *Inorg. Chem.* **2018**, *57*, 12338-12346.

(40) Mousavi, M.; Duhayon, C.; Béreau, V.; Guionneau, P.; Sutter, J.-P. First Magnets Based on Thiocyanato-Bridges *Chem. Comm.* **2012**, *48*, 10028-10030.

(41) Skorupa, A.; Korybut-Daszkiewicz, B.; Mrozinski, J. Heteronuclear thiocyanate-bridged compounds of the type $(NiL)_3[M(NCS)_6]_2$ (M=Fe(III), Cr(III); L=5,6,12,13-Me4-[14]-4,11-dieneN4) *Inorg. Chim. Acta* **2002**, *336*, 65-70.

(42) Wrzeszcz, G.; Dobrzanska, L.; Wojtczak, A.; Grodzicki, A. Magnetostructural characterisation of the first bimetallic assemblies derived from the anionic building block $[Cr(NCS)_6]^{3-}$ $[M(en)_3]_n$-[{$M(en)_2$-μ-SCN-$Cr(NCS)_4$-μ-NCS}$_{2n}$] with M = Ni(II), Zn(II) *Dalton Trans* **2002**, 2862-2867.

(43) Cucos, A.; Avarvari, N.; Andruh, M.; Journaux, Y.; Müller, A.; Schmidtmann, M. Reinecke Anion Derivatives and Homobinuclear Complexes as Tectons in Designing Heteropolymetallic Systems *Eur. J. Inorg. Chem.* **2006**, 903-907.

(44) Gonzalez, R.; Acosta, A.; Chiozzone, R.; Kremer, C.; Armentano, D.; De Munno, G.; Julve, M.; Lloret, F.; Faus, J. New Family of Thiocyanate-Bridged Re(IV)-SCN-M(II) (M = Ni, Co, Fe, and Mn) Heterobimetallic Compounds: Synthesis, Crystal Structure, and Magnetic Properties *Inorg. Chem.* **2012**, *51*, 5737-5747.

(45) Mousavi, M.; Béreau, V.; Desplanches, C.; Duhayon, C.; Sutter, J.-P. Substantial exchange coupling for {Mo-NCS-M} combination: illustration for 1-D [{$Mo(NCS)_6$}{$NiL_2$(NCS)]$_n$ *Chem. Comm.* **2010**, *46*, 7519-7521.

(46) Pearson, R. G. Hard and Soft Acids and Bases *J. Am. Chem. Soc.* **1985**, *85*, 3533-3539.

(47) Schmidtke, H. H.; Garthoff, D. Preparation and characterization of some thiocyanate and selenocyane complexes of transition metals *Helv. Chim. Acta* **1967**, *50*, 1631-1638.

(48) *Handbook of Chemistry and Physics*; 85 ed.; Lide, D. R., Ed.; CRC Press: Boca Raton, 2005.

(49) Chilton, N. F.; Anderson, R. P.; Turner, L. D.; Soncini, A.; Murray, K. S. PHI *J. Comput. Chem.* **2013**, *34*, 1164 – 1175.

(50) Drillon, M.; Coronado, E.; Beltran, D.; Georges, R. Classical treatment of a Heisenberg linear chain wiyh spin alternation; application to the MnNi(EDTA)-$6H_2O$ complex *Chem. Phys.* **1983**, *79*.

(51) Kahn, O. *Molecular Magnetism*; VCH: Weinheim, 1993 (page 38).

(52) Long, K. M.; Busch, D. H. Cobalt(II) complexes of quadridentate macrocycle 2,12-dimethyl-3,7,11,17-tetraazabicyclo[11.3.1]heptadeca-1(17),2,11,13,15-pentaene *Inorg. Chem.* **1970**, *9*, 505-512.

(53) Carlin, R., L. *Magnetochemistry*; Springer-Verlag: Berlin Heidelberg, **1986**.

(54) Palion-Gazda, J.; Machura, B.; Lloret, F.; Julve, M. Ferromagnetic Coupling Through the End-to-End Thiocyanate Bridge in Cobalt(II) and Nickel(II) Chains *Cryst. Growth Des.* **2015**, *15*, 2380-2388.

(55) Monfort, M.; Bastos, C.; Diaz, C.; Ribas, J.; Solans, X. Crystal structure and magnetic properties of the first 1D nickel(II) complex with bridging thiocyanato ligands in cis position: {catena-(μN,S-NCS)[$Ni(en)_2$]}($PF_6$) *Inorg. Chim. Acta* **1994**, *218*, 185-188.

(56) Boeckmann, J.; Näther, C. A rational route to SCM materials based on a 1-D cobalt selenocyanato coordination polymer *Chem. Comm.* **2011**, *47*, 7104-7106.

(57) Neumann, T.; Rams, M.; Tomkowicz, Z.; Jess, I.; Näther, C. Tuning of the exchange interaction and the Curie temperature by mixed crystal formation of the bridging anionic ligands *Chem. Comm.* **2019**, *55*, 2652-2655.

(58) Rojo, T.; Cortés, R.; Lezama, L.; Arriortua, M. I.; Urtiaga, K.; Villeneuve, G. Spectroscopic and magnetic properties of two ferromagnetically coupled nickel(II) dimers [{Ni(terpy)(NCX)$_2$}$_2$](terpy = 2,2′ :6′,2″-terpyridine, X = S or Se). Crystal structure of the thiocyanate *J. Chem. Soc. Dalton Trans.* **1991**, 1779-1783.

(59) Duggan, D. M.; Hendrickson, D. N. Magnetic exchange interactions in transition metal dimers. III. Nickel(II) di-μ-cyanato, di-μ-thiocyanato, and di-μ-selenocyanato complexes and related outer-sphere copper(II) complexes *Inorg. Chem.* **1974**, *13*, 2929-2940.

(60) Soares, A. B.; Taylor, R. S.; Sykes, A. G. Hexachloroiridate(IV) oxidation of hexathiocyanatomolybdate(III). Formation of molybdenum(IV) and identification of an aquation step prior to oxidation to molybdenum(V) *Inorg. Chem.* **1978**, *17*, 496-498.

(61) State, H. M. In *Inorg. Synth.*; Rochow, E. G., Ed. 1960; Vol. 6, pp. 198-199s.

(62) Poon, C. K.; Wan, W. K.; Liao, D. Structural and mechanistic studies of co-ordination compounds. Part 17. Preparation and acid hydrolysis of some cobalt(III) complexes containing the quadridentate macrocycle 2,7,12-trimethyl-3,7,11,17-tetra-azabicyclo[11.3.1] heptadeca-1 (17),2,11,13,15-pentaene: an extra-ordinary hydrolysis reaction *J. Chem. Soc., Dalton Trans.* **1977**, *13*, 1247-1251.

(63) Karn, J. L.; Busch, D. H. *Inorg. Chem.* **1969**, *8*, 1149-1153.

(64) Sabatini, A.; Bertini, I. Infrared Spectra between 100 and 2500 cm$^{-1}$ of Some Complex Metal Cyanates, Thiocyanates, and Selenocyanates *Inorg. Chem.* **1965**, *4*, 959-961.

(65) Author list given in SI; Gaussian, Inc.: Pittsburgh, PA, 2004

(66) Lee, C.; Yang, W.; Parr, R. G. Development of the Colle-Salvetti correlation-energy formula into a functional of the electron density *Phys. Rev. B: Condens. Matter* **1988**, *37*, 785-789.

(67) Becke, A. D. J. Density-functional thermochemistry. III. The role of exact exchange *J. Chem. Phys.* **1993**, *98*, 5648-5652.

(68) Dunning, T. H. J.; Hay, P. J. Modern Theoritical Chemistry **1976**, *3*, Plenim, New-York.

(69) Hay, P. J.; Wadt, W. R. Ab initio effective core potentials for molecular calculations. Potentials for the transition metal atoms Sc to Hg *J. Chem. Phys.* **1985**, *82*, 270-283.

(70) Hay, P. J.; Wadt, W. R. Ab initio effective core potentials for molecular calculations. Potentials for K to Au including the outermost core orbitals *J. Chem. Phys.* **1985**, *82*, 299-310.

(71) Wadt, W. R.; Hay, P. J. Ab initio effective core potentials for molecular calculations. Potentials for main group elements Na to Bi *J. Chem. Phys.* **1985**, *82*, 284-298.

(72) Altomare, A.; Cascarano, G.; Giacovazzo, C.; Guargliardi, A.; Burla, M. C.; Polidori, G.; Camalli, M. SIR92 *J. Appl. Crystallogr.* **1994**, *27*, 435.

(73) Sheldrick, G. M. Crystal structure refinement with SHELXL *Acta Cryst.* **2015**, *C71*, 3-8.

(74) Palatinus, L.; Chapuis, G. Superflip *J. Appl. Crystallogr.* **2007**, *40*, 786-790.

(75) Betteridge, P. W.; Carruthers, J. R.; Cooper, R. I.; Prout, K.; Watkin, D. J. CRYSTALS *J. Appl. Crystallogr.* **2003**, *36*, 1487-1487.

(76) Spek, A. L. PLATON SQUEEZE: a tool for the calculation of the disordered solvent contribution to the calculated structure factors *Acta Cryst.* **2015**, *C71*, 9-18.

# Molybdenum(III) Thiocyanate- and Selenocyanate-Based 1D-Heteronuclear Polymers: Coordination Affinity-Controlled Assemblage of Mixed Spin and Mixed Valence Derivatives with Ni(II) and Co(II/III)

---

**Scheme S1**. Sketch of macrocyclic ligand 2,12-dimethyl-3,7,11,1-tetraazabicyclo [11.3.1]-heptadeca-1(17),2,11,13,15-pentaene, $L^{N4}$.

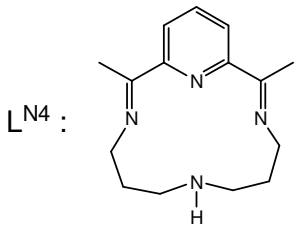


**Figure S1.** 1D-[{Mo(NCS)$_6$}{Ni(en)$_2$}]·0.5{Ni(en)$_3$} $H_2O$, **1** : ORTEP view of the asymmetric unit. Selected bond lengths (Å) and angles (°) patterning to the anionic units: distances (Å) Mo1-N2, 2.088(5); Mo1-N1, 2.096(5); Ni1*-S2, 2.578(2); Ni1-S1 = 2.624(1); angles (°) Ni1-S2-C2, 104.54(18); Ni1-S1-C1, 92.109(17); Mo1-N1-C1, 171.995(42); Mo1-N2-C2, 172.770(40). H atoms are not shown. Symmetry: *, *x,-y,-0.5+z*.

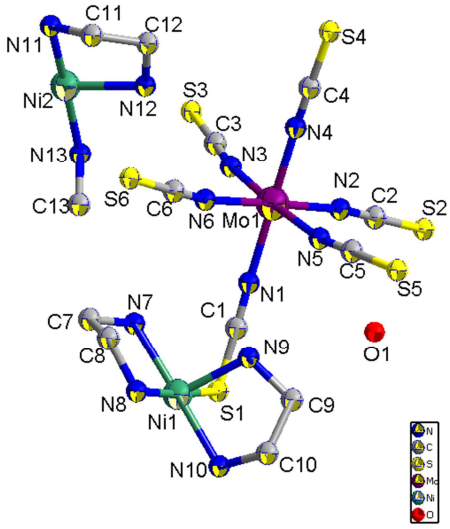

**Figure S2** Crystal packing for **1**. (right) Close contacts between chains; the shortest S···S separations are materialized by dotted lines. Distances (Å): S2···S2, 3.92; S2···S3, 3.73; S4···S3, 3.72.

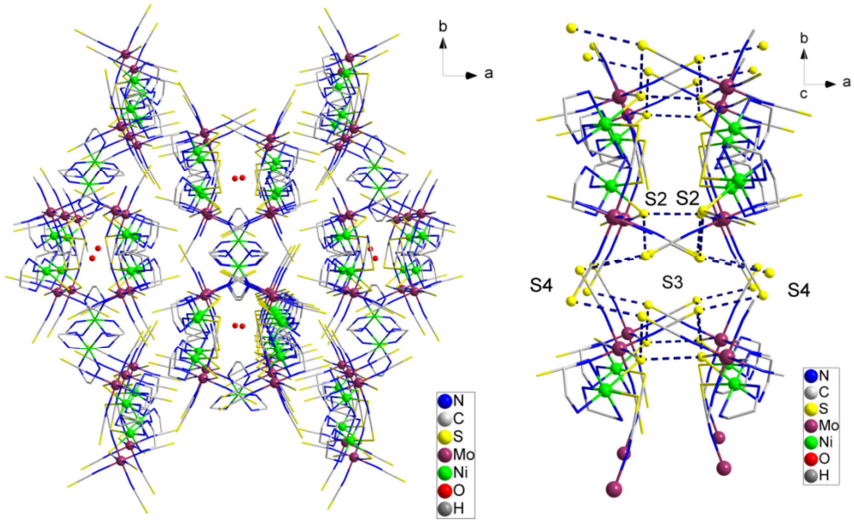


**Figure S3.** 1D-[{Mo(NCS)$_6$}{NiL$^{N4}$}]·0.5{NiL$^{N4}$(CH$_3$CN)$_2$}·0.5CH$_3$CN·H$_2$O, **2**: ORTEP view of the two asymmetric units.

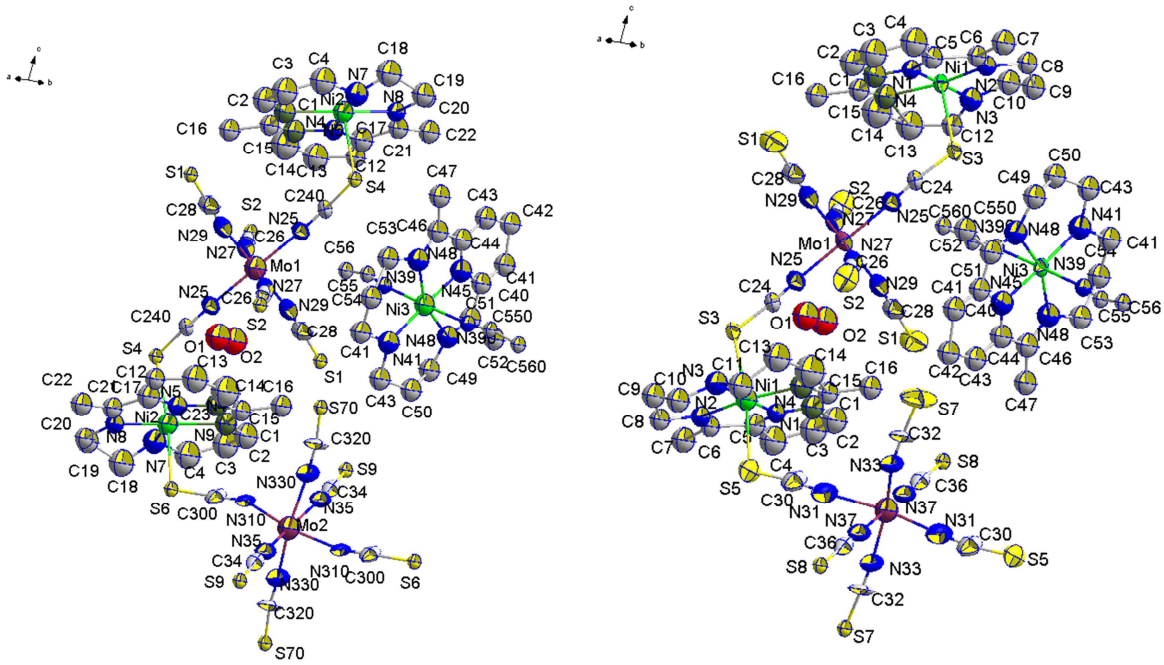

The structure for **2** presents a statistic disorder that concerns most of the atoms; a short description of the situation is given below. Diffraction data were collected on several crystals from different batches. The same cell parameters were obtained, leading to the same structure with the same

disorders. Careful examination of the reciprocal lattice didn't permit to get other cell parameters. Refinement of the final formulated model leads to an imperfect but reasonable solution.

Oddly, Mo2 is not located on the special position (0, 1, 0.5), as a result Mo resides on two positions with a partial occupancy. The thiocyanates with partial occupancy were located for each Mo position.

The Nickel atom is also located on two positions with partial occupation (Ni1 and Ni2). Each Ni is surrounded by its ligand which is present in full in the asymmetric unit. Some atoms (C2 C3 C4 C13 C14 C15 C16) are common to the two ligands (occupancy 1). Other atoms have partial occupancy whereas C23/N4 and C1/N9 have mixed positions.

A view of this situation is depicted in (a) below.

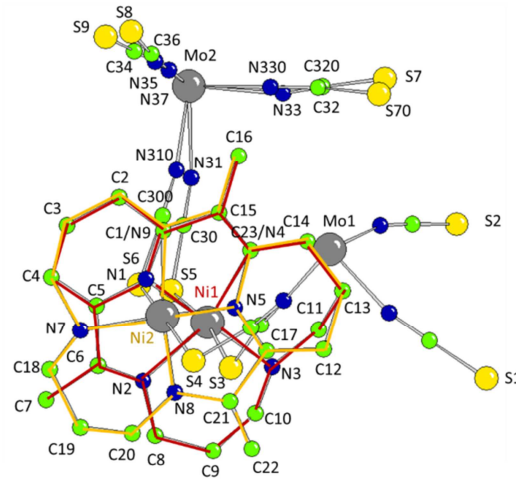


**(a)**

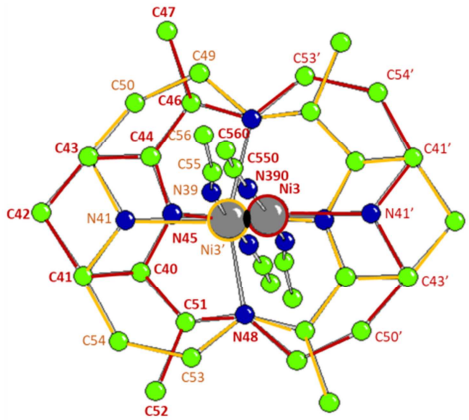


**(b)**

For the discrete fragment: Ni3 has a half occupancy and is located at 0.4 Å from the inversion center (-0.5, 1, 1). Ni3' is generated by the symmetry center. The atomic positions of the ligand around Ni3 and Ni3' were located by Fourrier difference. Most of the atoms have occupancy 0.5 (belonging to one of the 2 parts of the ligand). 3 atoms (N48, C41 and C43) have occupancy 1 (belonging to the 2 parts of the ligand). A view of a whole complex after symmetry what applied is given in (b) above.

**Figure S4.** 1D-[{Mo(NCS)$_6$}{NiL$^{N4}$}]·{Co$^{III}$L$^{N4}$Br$_2$}·CH$_3$CN, **3**: ORTEP view of the asymmetric unit. Selected bond lengths (Å) and angles (°): distances (Å) Co1-Br1, 2.413(2); Co1-Br2, 2.381(2); Ni1-S2, 2.561(2); Ni1-S1, 2.645(2); Mo1-N2, 2.083(5); Mo1-N1, 2.114(5); angles (°) Ni1-S2-C2, 108.65(2); Ni1-S1-C1,103.27(2); Mo1-N1-C1, 167.810(43); Mo1-N2-C2, 176.279(43); Br1-Co1-Br2, 179.710(75).

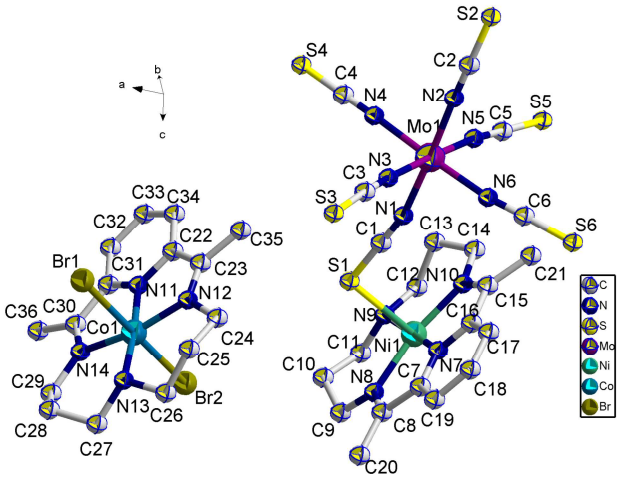


**Figure S5.** 1D-[{Mo(NCS)$_6$}{CoL$^{N4}$}]·{Co$^{III}$L$^{N4}$Br$_2$}·CH$_3$CN, **4**: ORTEP view of the asymmetric unit.

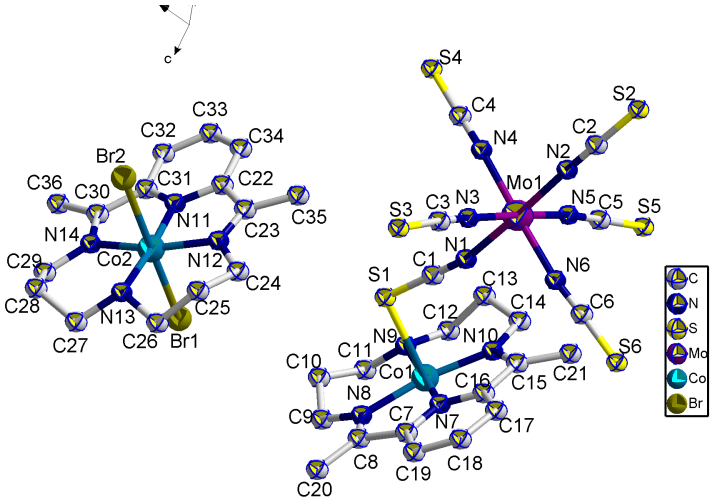


Selected bond distances (Å) and angles (°):

| | | | | | | |
|---|---|---|---|---|---|---|
| Co1 | N7 | 1.8286(84) | Co1 | S1 | C1 | 102.6(3) |
| | N10 | 1.9338(64) | Co1 | N2 | C2 | 108.4(2) |
| | N9 | 1.9830(84) | Mo1 | N1 | C1 | 167.9(6) |
| | N8 | 1.9838(70) | Mo1 | N2 | C2 | 176.4(6) |
| | S2 | 2.5767(25) | | | | |
| | S1 | 2.6897(26) | | | | |
| Co2 | N11 | 1.8406(59) | Br1 | Co2 | Br2 | 179.66(7) |
| | N12 | 1.9420(63) | | | | |
| | N13 | 1.9741(86) | | | | |

N14 1.9888(68)

**Figure S6.** Detail of the π–π stacking between chains in **3** and **4**. Distances between the centroids of the pyridine units: in **3** for $NiL^{N4}$ and $Co^{II}L^{N4}Br_2$: 4.078 (Å); $NiL^{N4}$ and $NiL^{N4}$: 4.008 (Å); in **4** $Co^{(II)}L^{N4}$ / $Co^{(III)}L^{N4}Br_2$, 4.093 (Å), and $Co^{(II)}L^{N4}$ / $Co^{(II)}L^{N4}$, 4.027 (Å).

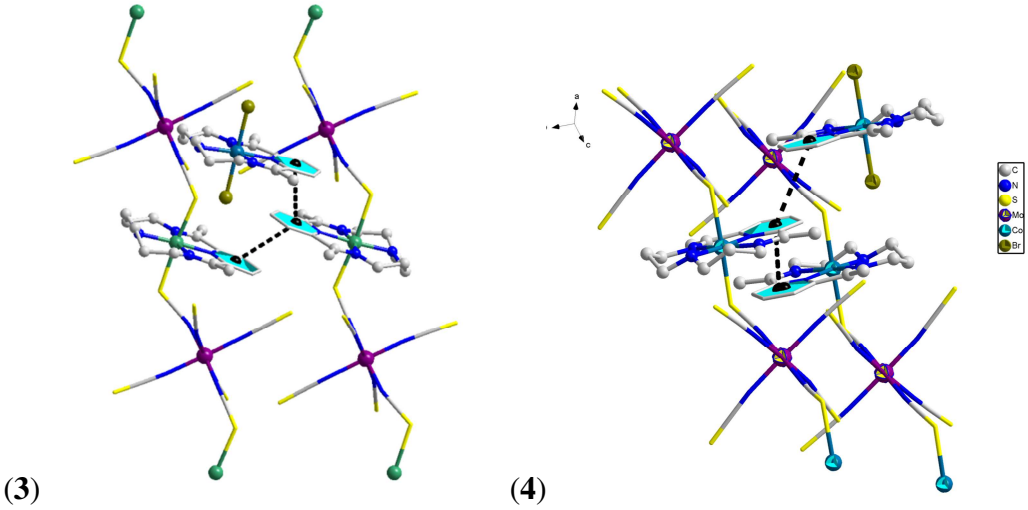


(**3**) (**4**)

**Figure S7.** 1D-[{Mo(NCS)$_6$}{CoL$^{N4}$}$_2$(NCS)]·CH$_3$CN, **5**: (*left*) ORTEP view of the asymmetric unit at $T$ = 110 K and (*right*) superposition of the asymmetric units at $T$ = 273 K (ellipsoids at the 30% probability level) and 100K (ball and sticks in green). This last drawing is the inverted image of the actual structure to have the same enantiomer as that of the crystal collected at 273 K.

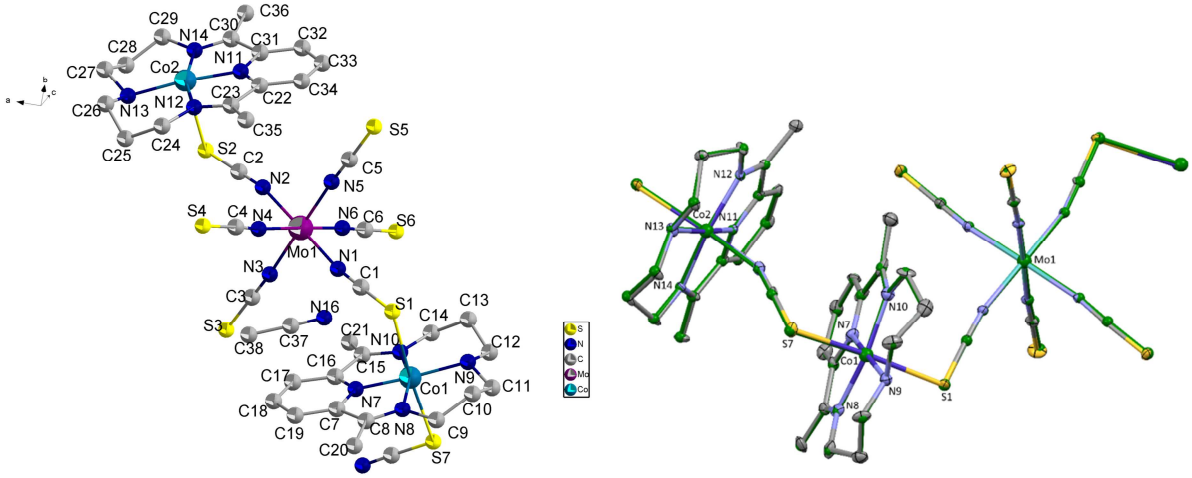


Selected bond distances (Å) and angles (°):

| | | | $T$ = 100K | $T$ = 273K |
|---|---|---|---|---|
| Co1 | N7 | | 1.839(6) | 1.840(4) |
| | N10 | | 1.910(5) | 1.921(4) |
| | N9 | | 1.987(5) | 1.981(4) |
| | N8 | | 2.019(5) | 2.014(4) |
| | S7 | | 2.563(2) | 2.590(1) |
| | S1 | | 2.632(2) | 2.670(1) |
| Co2 | N11 | | 1.854(5) | 1.844(4) |
| | N12 | | 1.962(5) | 1.943(4) |
| | N13 | | 1.982(5) | 1.977(4) |
| | N14 | | 1.985(4) | 1.997(4) |
| | N15 | | 2.146(5) | 2.161(4) |
| | S2 | | 2.710(2) | 2.757(2) |
| | | | **110 K** | **273 K** |
| C1 | S1 | Co1 | 103.7(2)° | 104.3(1)° |

| | | | | |
|---|---|---|---|---|
| C46 | S7 | Co1 | 102.0(2) | 101.7(1)° |
| C2 | S2 | Co2* | 104.5(2)° | 105.1(1)° |
| C1 | N1 | Mo1 | 169.5(4)° | 169.5(3)° |
| C2 | N2 | Mo1 | 166.6(4)° | 167.2(3)° |
| C3 | N3 | Mo1 | 173.3(5)° | 173.7(4)° |
| C4 | N4 | Mo1 | 177.0(4)° | 176.5(4)° |
| C5 | N5 | Mo1 | 172.6(4)° | 173.2(3)° |
| C6 | N6 | Mo1 | 177.0(4)° | 176.1(4)° |

*, *-x,-0.5+y,1-z*

**Figure S8.** ORTEP view of the asymmetric unit of $[PPh_4]_3\{Mo(NCSe)_6\}\cdot CH_3CN$. Selected bond lengths (Å) and angles (°) patterning to the anionic units: Mo-N, (range) 2.095(2) to 2.115(2); N-C, (range) 1.154(3) to 1.161(3); C-Se, (range) 1.770(3) to 1.784(3) ; Mo-N1-C1, 175.7(2); Mo-N2-C2, 175.4(2); Mo-N3-C3, 174.2(2); Mo-N4-C4, 172.7(2); Mo-N5-C5, 172.7(2); Mo-N6-C6, 171.1(2)°.

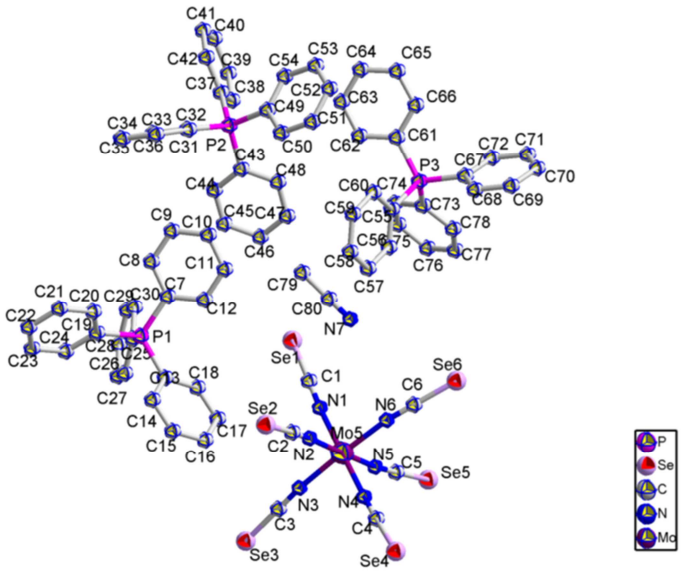


**Figure S9.** Ladder type organization of the $\{Mo(NCSe)_6\}^{3-}$ complexes in the crystal of $(PPh_4)_3\{Mo(NCSe)_6\}\cdot CH_3CN$, the shortest Se···Se separations are materialized by dotted lines. Distances: Se1···Se4(-1+x, y, z), 3.7502(4) Å; Se2···Se2(2-x, 1-y, 1-z), 3.3757(4) Å ; Se4···Se1(1+x, y, z), 3.7502(4) Å.

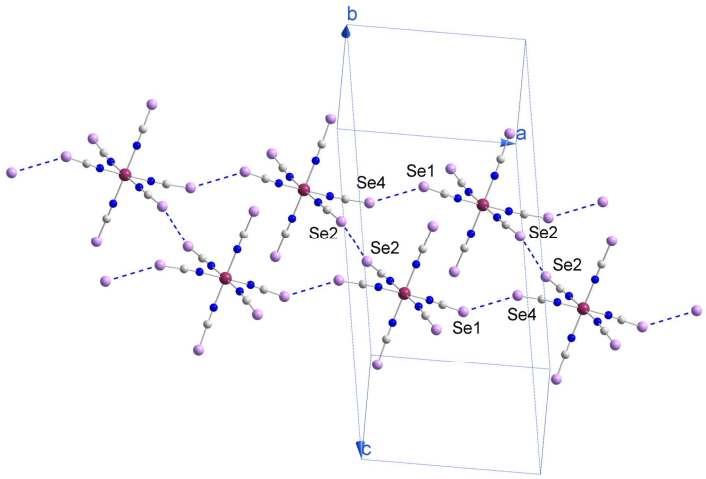

**Figure S10** 1D-[{Mo(NCSe)$_6$}{NiL$^{N4}$}$_2$(NCS)]·CH$_3$CN, **6**: ORTEP view of the asymmetric unit and crystal packing. Selected geometric data: distances (Å) Ni1-Se1, 2.6769(9); Ni2-Se2, 2.7614(9); Ni1-S1, 2.552(1); Ni2-N15, 2.105(5); Mo-N, 2.084(5)-2.109(4); angles (°) Ni1-Se1-C1, 101.6(1); Ni2-Se2-C2, 103.3(2); Ni1-S1-C46, 103.5(2); Mo-N-C, 166.7(4)-177.2(4); Ni2-N15-C46, 155.2(4).

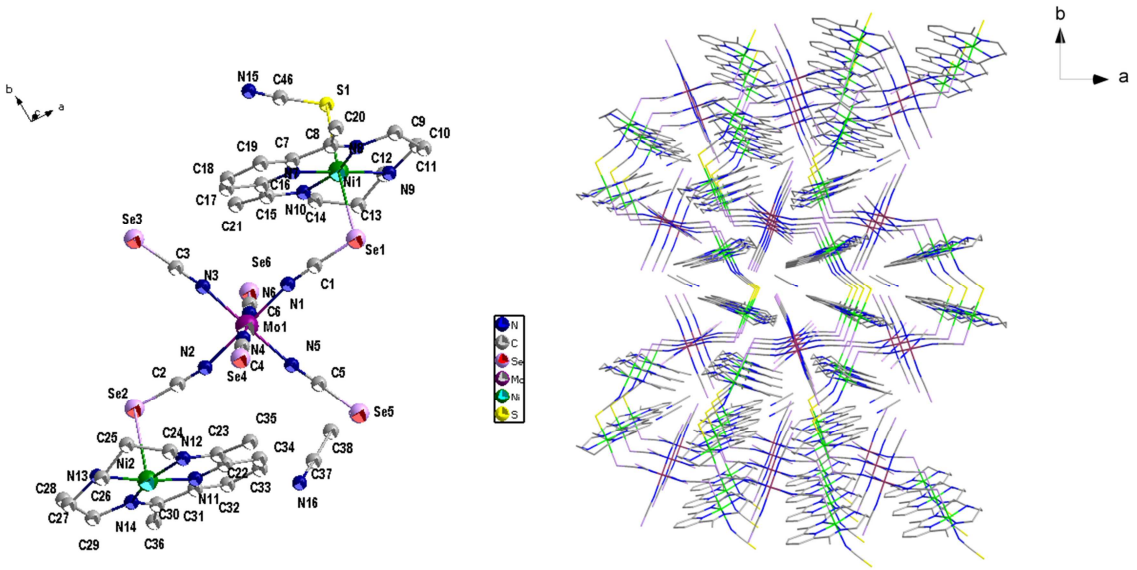


**Table S1** Spin density distribution in [Mo(NCSe)$_6$]$^{3-}$

| N | C | Se | Mo | |
|---|---|---|---|---|
| -0.081242 | 0.097615 | 0.067972 | 2.474089 | |
| -0.074613 | 0.089112 | 0.061708 | | |
| -0.079583 | 0.099643 | 0.06752 | | |
| -0.08283 | 0.104667 | 0.069896 | | |
| -0.086303 | 0.107056 | 0.072968 | | |
| -0.084777 | 0.103674 | 0.073428 | | |
| -0.081558 | 0.1002945 | 0.06891533 | mean | |
| | | | | |
| -0.05817946 | 0.11149664 | 0.10458243 | (MEAN-MIN)/MEAN | |
| -0.08515412 | 0.06741646 | 0.06548132 | (MAX-MEAN)/MEAN | |

**Figure S11** Experimental (o) and calculated (–) $\chi_M T$ versus $T$ and $M$ versus $H$ (2 K) behavior for $[PPh_4]_3\{Mo(NCSe\}_6 \cdot CH_3CN$. Best fit parameters: $g$ = 1.9290 ± 0.0008, $D$ = 3.7 ± 0.1 $cm^{-1}$ and $zJ'$ = -0.117 ± 0.03 $cm^{-1}$.

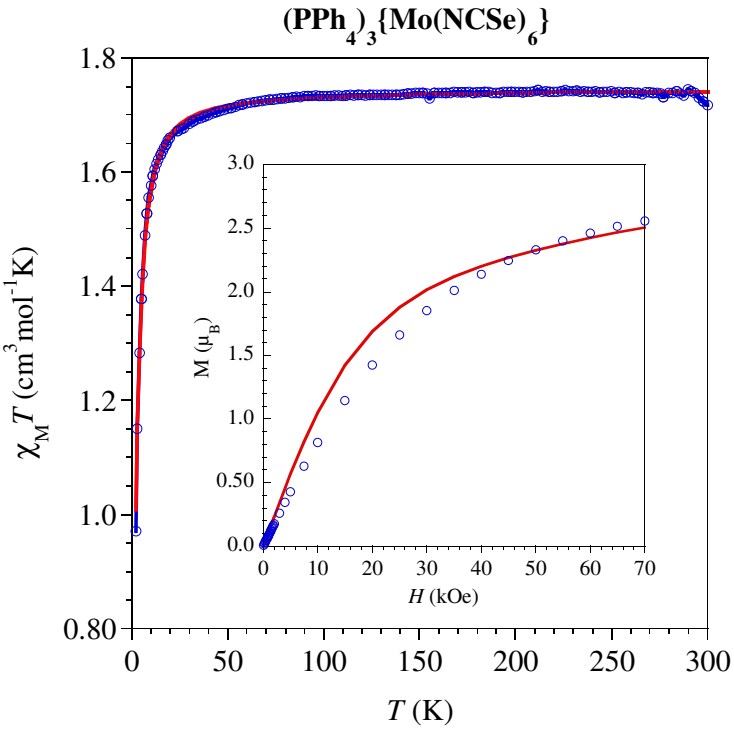


**Figure S12** Field dependence of the magnetization for **1**, at 2K. The solid lines is a guide for the eyes.

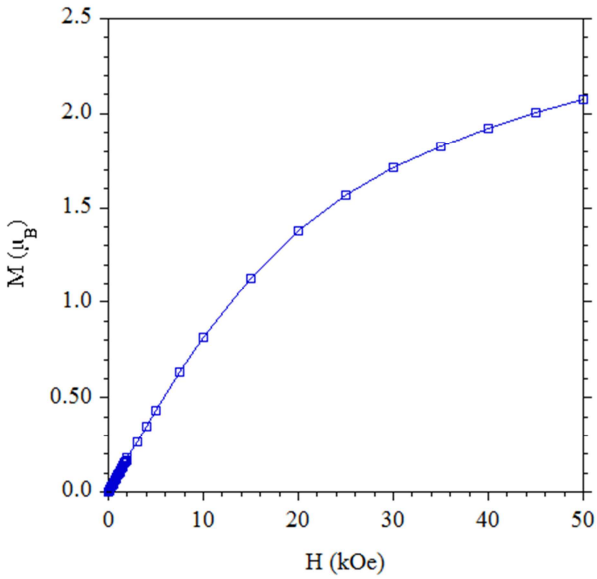

**Figure S13** Field dependence of the magnetization for **2**, at 2K. The solid lines is a guide for the eyes.

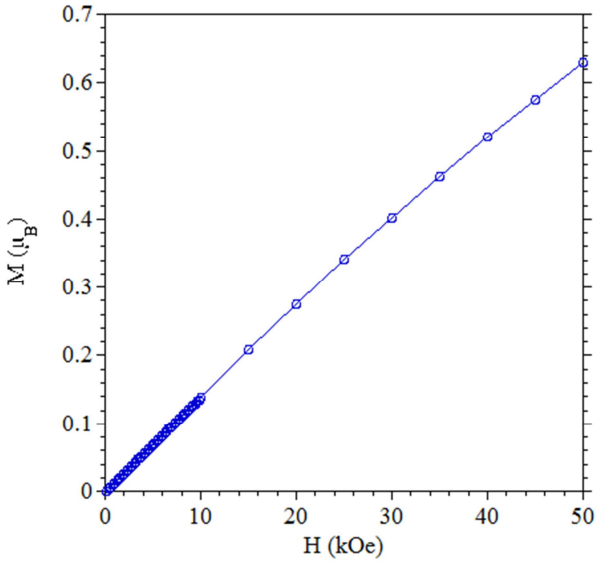


**Figure S14**: Compound **3**: *(left)* $\chi_M = f(T)$, and *(right)* field dependence of the magnetization for **3**, at 2K. The solid lines are guides for the eyes.

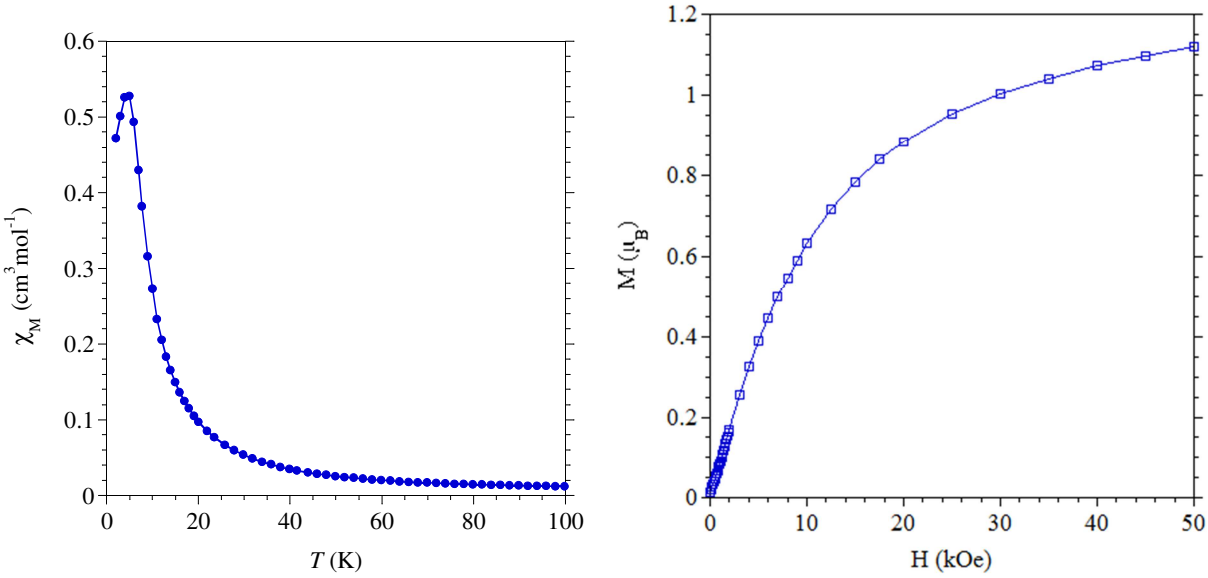

**Figure S15.** Compound **4**: *(a)* $\chi_M = f(T)$, and *(b)* field dependence of the magnetization at 2K (blue line) and 10K (black line); the solid lines are guides for the eyes. (c) AC susceptibility recorded with $H_{AC}$ = 3 Oe at a frequency of 100 Hz, in zero field (blue) and in an applied DC field of 8 kOe (red).

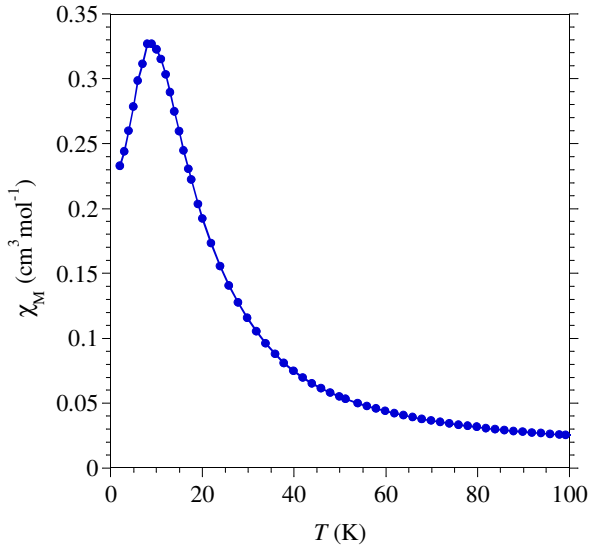


*(a)*

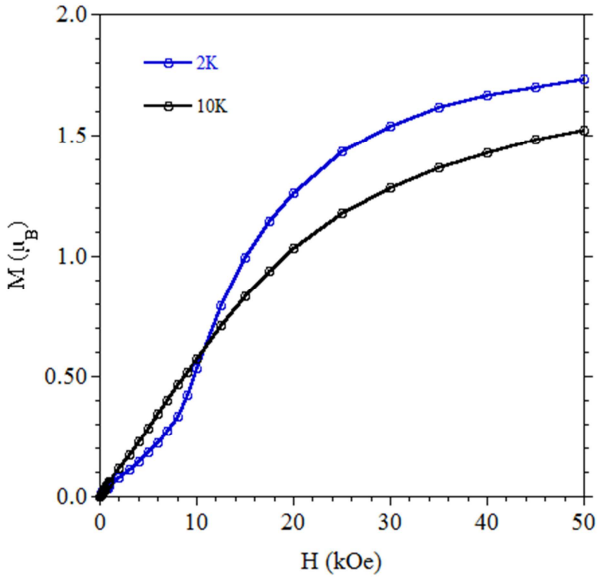


*(b)*

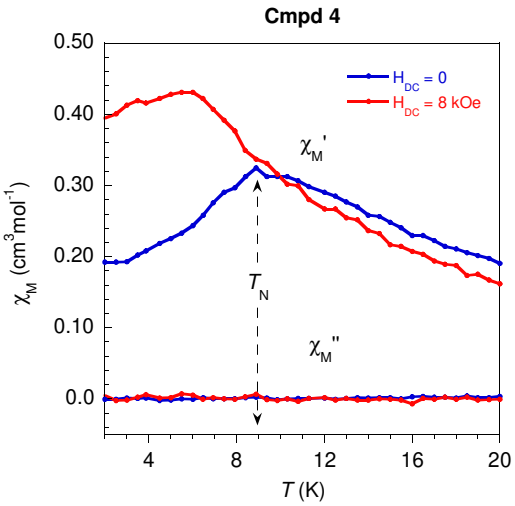


*(c)*

**Figure S16** Field dependence of the magnetization for **5**. The solid lines are guides for the eyes.

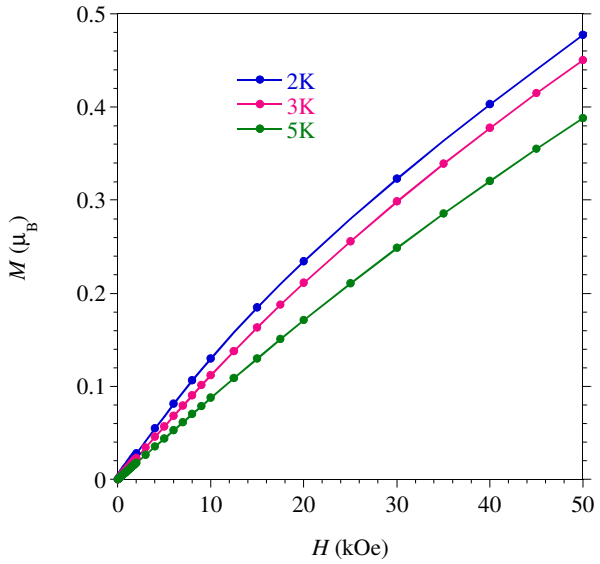


**Figure S17** Field dependence of the magnetization for **6**, at 2K. The solid line is a guide for the eyes.

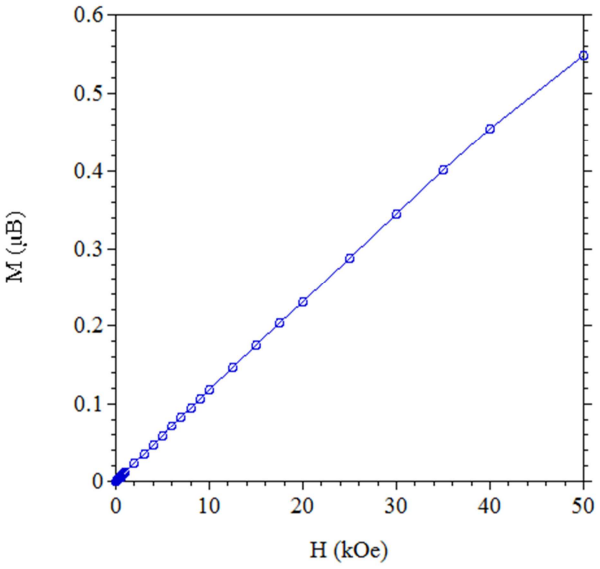

**Figure S18.** Magnetic behaviour for $[CoL^{N4}(H_2O)_2](ClO_4)_2$. The solid line is a guide for the eyes.

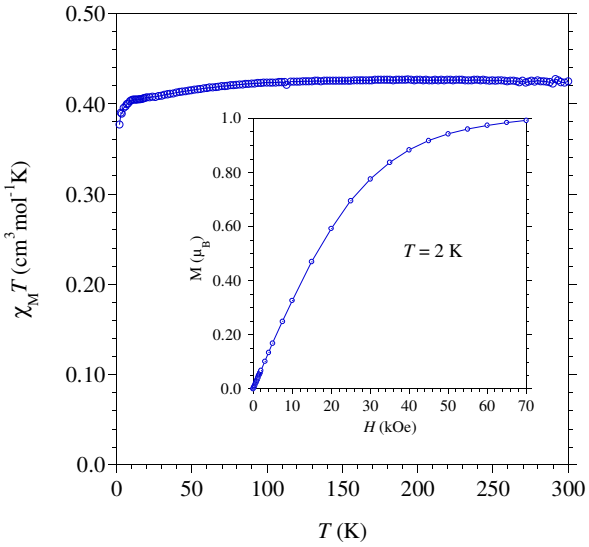

**Figure S19.** Powder X-Ray patterns for **2**-**5**. In the plots the blue line (up) is the experimental diffractogram obtained from the crystals batch and the red line (down) the calculated diffractogram from the single crystal X-Ray diffraction.

[{Mo(NCS)$_6$}{NiL$^{N4}$}]·0.5[NiL$^{N4}$(MeCN)$_2$], **2**

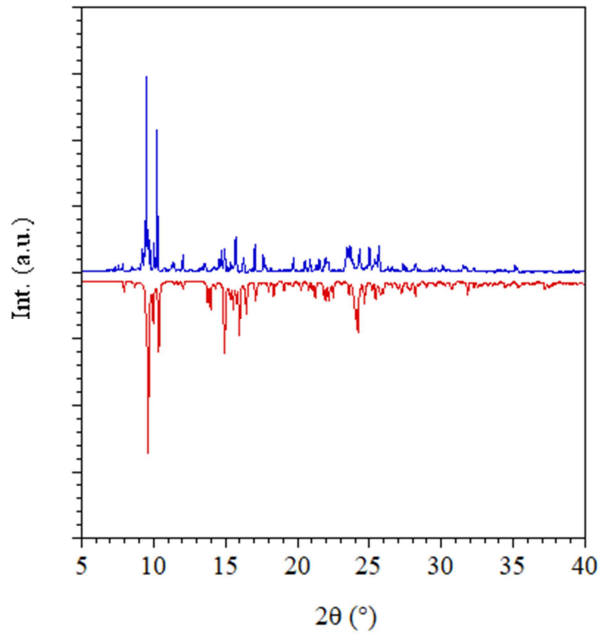


[{Mo(NCS)$_6$}{NiL$^{N4}$}][Co$^{III}$L$^{N4}$Br$_2$], **3**

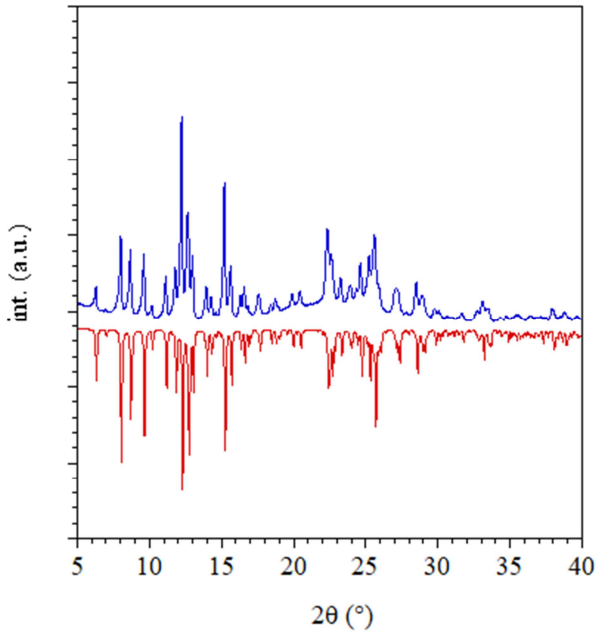


[{Mo(NCS)$_6$}{Co$^{II}$L$^{N4}$}][Co$^{III}$L$^{N4}$Br$_2$], **4**

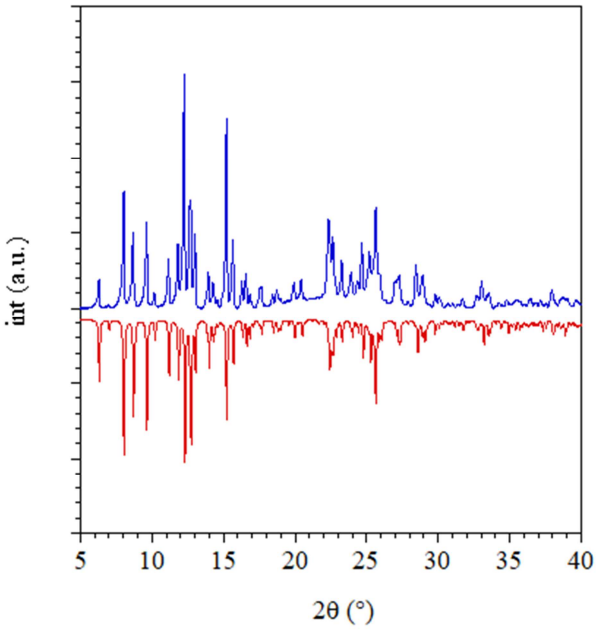


[{Mo(NCS)$_6$}{Co$^{II}$L$^{N4}$}$_2$(NCS)], **5**

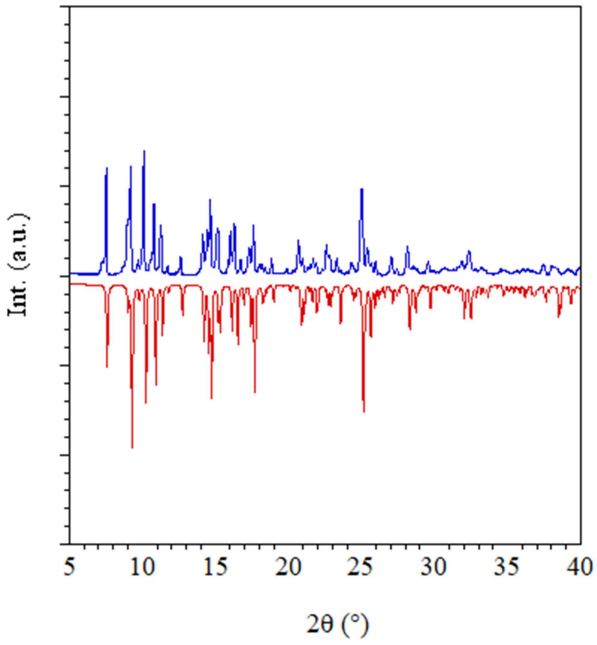

**Gaussian reference:**

Gaussian 03, M. J. Frisch, G. W. Trucks, H. B. Schlegel, G. E. Scuseria, M. A. Robb, J. R. Cheeseman, G. Scalmani, V. Barone, G. A. Petersson, H. Nakatsuji, X. Li, M. Caricato, A. Marenich, J. Bloino, B. G. Janesko, R. Gomperts, B. Mennucci, H. P. Hratchian, J. V. Ortiz, A. F. Izmaylov, J. L. Sonnenberg, D. Williams-Young, F. Ding, F. Lipparini, F. Egidi, J. Goings, B. Peng, A. Petrone, T. Henderson, D. Ranasinghe, V. G. Zakrzewski, J. Gao, N. Rega, G. Zheng, W. Liang, M. Hada, M. Ehara, K. Toyota, R. Fukuda, J. Hasegawa, M. Ishida, T. Nakajima, Y. Honda, O. Kitao, H. Nakai, T. Vreven, K. Throssell, J. A. Montgomery, Jr., J. E. Peralta, F. Ogliaro, M. Bearpark, J. J. Heyd, E. Brothers, K. N. Kudin, V. N. Staroverov, T. Keith, R. Kobayashi, J. Normand, K. Raghavachari, A. Rendell, J. C. Burant, S. S. Iyengar, J. Tomasi, M. Cossi, J. M. Millam, M. Klene, C. Adamo, R. Cammi, J. W. Ochterski, R. L. Martin, K. Morokuma, O. Farkas, J. B. Foresman, and D. J. Fox, Gaussian, Inc., Wallingford CT, **2004**.